

Abstract

Multiple Sclerosis (MS) is a chronic neurodegenerative disorder characterized by demyelinating lesions in the central nervous system. Accurate and early diagnosis remains challenging due to the disease's complex and heterogeneous nature. This thesis proposes **MSFusionXAI**, an intelligent multimodal framework integrating **FLAIR MRI imaging**, clinical data, and explainable artificial intelligence (XAI) techniques for automated MS detection and interpretation.

The framework combines a deep learning based lesion segmentation model (**ResNet34-UNet**) with an **adaptive attention-guided fusion module** that jointly analyzes imaging features and clinical biomarkers (age, sex, EDSS, oligoclonal band status). The fused representation enables patient-level classification with **conditional branching logic**: subjects predicted as healthy terminate processing immediately, while MS predictions trigger automated lesion segmentation and quantification. A **BioBERT-based explainability module** generates structured natural language reports integrating attention weight distributions, lesion burden metrics, and clinical correlations.

The proposed architecture was evaluated on a clinical dataset from CHU Sahloul University Hospital (46 MS patients, 46 healthy controls) using rigorous five-fold stratified cross-validation. The multimodal fusion model achieved **93.7% classification accuracy** ($\pm 2.2\%$ std), substantially outperforming MRI-only (72.6%) and clinical-only (89.4%) baselines. Lesion segmentation reached a **Dice similarity coefficient of 0.823** with 76.4% sensitivity and 93.3% specificity on held-out test data. Attention weight analysis validated clinically meaningful modality prioritization, with MS patients exhibiting significantly higher MRI attention (0.64 ± 0.18) compared to healthy controls (0.42 ± 0.22 , $p < 0.001$).

Beyond quantitative results, a key contribution of this work lies in its interpretability. The integration of explainable AI enables the automatic generation of textual summaries highlighting lesion regions and their correlation with disease severity, thereby bridging the gap between deep learning predictions and clinical reasoning.

This thesis demonstrates that combining heterogeneous data modalities within a transparent AI framework can significantly enhance both the accuracy and trustworthiness of MS diagnosis, paving the way for future clinical decision-support systems based on explainable multimodal intelligence.

Dedication

Above all, I dedicate this study to our Almighty God, who granted me strength, knowledge, and guidance throughout this journey.

To my beloved parents, to whom I owe everything, for their constant sacrifices, love, and encouragement that have allowed me to pursue my dreams. This work is offered to them in gratitude for providing a peaceful and nurturing environment essential for the completion of this thesis.

To my dear Sabrine, Mouayed, and Khalil, whose love and encouragement have been my anchor throughout this journey. Your belief in me has been an endless source of strength and inspiration.

A heartfelt thank you goes to all my professors and mentors who guided me through every step of this project, offering invaluable advice and wisdom.

My deep respect and gratitude extend to all those who have contributed, even in the smallest way, to the realization of this research.

Thank you all.

- Syrine

Acknowledgment

First and foremost, I would like to express my sincere gratitude to my academic supervisor, **Dr. Dalel Kanzari**, for her invaluable guidance, insightful feedback, and continuous encouragement throughout the development of this thesis. Her expertise and dedication have been instrumental in shaping the quality and direction of this work.

I would also like to extend my heartfelt thanks to my research supervisors, **Pr. Sana Ben Amor** and **Dr. Ahmed Mili** (CHU of Sahloul, Sousse), for their support, advice, and collaboration, which were essential in bridging the gap between medical expertise and artificial intelligence.

I am grateful to all the members of **Sahloul Hospital** and the collaborating research teams for providing access to clinical data and for their professional assistance during the evaluation phase.

My deepest appreciation goes to my professors and colleagues at the **Higher Institute of Applied Science and Technology of Sousse**, whose constructive discussions and helpful suggestions have enriched my research journey.

Finally, I would like to express my sincere gratitude to my family and friends for their unconditional love, patience, and belief in me. Their moral support has been the foundation of my perseverance throughout this challenging yet rewarding experience.

Contents

Abstract	I
Dedication	II
Acknowledgment	III
Acronyms	X
General Introduction	1
1 Background Concepts	3
1.1 Introduction	3
1.2 Medical Concepts	3
1.2.1 Multiple Sclerosis (MS)	3
1.2.2 Causes and Symptoms	4
1.2.3 Stages of Multiple Sclerosis	5
1.2.4 MS Detection Methods	6
1.2.5 Limitations of MS Detection Methods	8
1.3 Computer Science Concepts	9
1.3.1 Data Preprocessing	9
1.3.2 Artificial Intelligence	12
1.3.3 Data Integration	18
1.3.4 Explainable Artificial Intelligence (XAI)	18
1.4 Conclusion	19
2 State-Of-The-Art in Multimodal MS Detection	20
2.1 Introduction	20
2.1.1 Multimodal Data in MS Detection	20
2.1.2 Machine Learning and Deep Learning in Multimodal MS Analysis .	22
2.1.3 Explainability in AI Models for MS Detection	24
2.2 Comparative Analysis	25
2.2.1 Assessment of Related Works	27
2.3 Research Motivation and Objective	28
2.4 Conclusion	28
3 Proposed Method: MSFusionXAI	30
3.1 Introduction	30
3.2 System Overview	30

Contents

3.3	Dataset Description	31
3.3.1	Cohort Composition	31
3.4	MRI Preprocessing Pipeline	31
3.4.1	Orientation Standardization & Rotation Correction:	32
3.4.2	Bias Field Correction:	32
3.4.3	Skull Stripping:	32
3.4.4	Intensity Normalization:	32
3.4.5	Denoising:	32
3.4.6	Geometric Resampling:	33
3.4.7	Intensity Harmonization:	33
3.5	MRI Feature Extraction (CNN Encoder)	33
3.5.1	Network Architecture	33
3.5.2	Training Strategy	34
3.6	Clinical Feature Extraction (MLP Encoder)	34
3.6.1	Feature Encoding & Normalization	34
3.6.2	MLP Architecture	34
3.7	Adaptive Attention-Based Fusion	35
3.7.1	Motivation and Architecture	35
3.8	Multimodal Classification	36
3.8.1	Training Strategy and Cross-Validation	36
3.8.2	Conditional Branching Logic	37
3.9	Lesion Segmentation Module (ResNet34U-Net)	38
3.9.1	Architecture	38
3.9.2	Training Strategy	38
3.9.3	Inference and Quantification	38
3.10	Explainability Module (XAI)	39
3.10.1	Attention-Based Explanations	39
3.10.2	Lesion Correlation Analysis	39
3.10.3	Natural-Language Report Generation	39
3.11	Implementation Details	40
3.12	Conclusion	40
4	Experiments, Results & Discussion	41
4.1	Introduction	41
4.2	Experimental Setup	41
4.2.1	Hardware and Software Environment	41
4.2.2	Dataset Split	41
4.2.3	Training Hyperparameters	42
4.2.4	Evaluation Metrics	42
4.3	Classification Results	43
4.3.1	Five-Fold Cross-Validation Results	43
4.3.2	Comparison: MRI-Only vs Clinical-Only vs Fusion	44
4.3.3	Confusion Matrix Analysis	45
4.3.4	Analysis of Variability Between Folds	45
4.4	Segmentation Results	46
4.4.1	Dice Score on Test Set	46

Contents

4.4.2	Sensitivity and Specificity	46
4.4.3	Lesion Volume Quantification	46
4.4.4	Qualitative Visualizations	47
4.5	Comparison with State-of-the-Art Segmentation Methods	48
4.6	Explainability Analysis	49
4.6.1	Attention Weight Analysis	49
4.6.2	Correlation Between Lesion Burden and MRI Attention	49
4.6.3	BioBERT-Generated Clinical Reports	50
4.6.4	Case Studies with Explainable Reports	52
4.6.5	Explainability Validation	52
4.7	Ablation Studies	53
4.7.1	Attention Fusion vs Simple Concatenation	53
4.7.2	Impact of Preprocessing Steps	53
4.7.3	Impact of Removing Clinical Features	53
4.8	Computational Efficiency	54
4.8.1	Training Time	54
4.8.2	Inference Time	54
4.9	Discussion	54
4.9.1	Interpretation of Results	54
4.9.2	Limitations	54
4.9.3	Clinical Implications	55
4.10	Conclusion	55
	General Conclusion and Future Work	56

List of Figures

1.1	Neuropathological changes in MS [81].	4
1.2	Multiple sclerosis subtypes [30]..	6
1.3	Raw MRI image (left) with visible bias field; corrected image (right) using N4ITK [82].	10
1.4	Skull-stripping steps in MRI preprocessing: (A) Original input image, (B) Brain tissue contouring, and (C) Removal of non-brain tissues [49].	10
1.5	Denoising results: (Top) Original noisy MRI, (Bottom) Denoised output [51].	11
1.6	Intensity normalization stages: Reference (top), input, histogram-matched, and WhiteStripe-normalized results [53].	11
1.7	Hierarchical overview of Artificial Intelligence techniques in Medical Diagnosis.	13
1.8	Architecture of a fully-connected neural network showing input, hidden, and output layers with weighted connections between neurons.	14
1.9	Typical architecture of a Convolutional Neural Network (CNN) showing convolution, activation, pooling, and fully connected layers[83].	15
1.10	DenseNet block illustration: each layer receives input from all previous layers, followed by a transition layer [61].	16
1.11	U-Net architecture: encoder-decoder structure with skip connections, showing convolution, pooling, up-convolution, and output segmentation map [32].	17
3.1	The MSFusionXAI pipeline architecture.	31
4.1	Performance comparison across four metrics for MRI-only (red), Clinical-only (blue), and Fusion (green) models averaged over five folds. Fusion achieves highest accuracy (91.2%) and F1-score (90. 2%).	45
4.2	Box plots showing distribution of segmentation metrics across seven test patients..	46
4.3	Representative segmentation example showing input FLAIR MRI (left), manual ground truth lesion mask by expert neurologist (center, red overlay), and U-Net predicted mask (right, green overlay).	47
4.4	Segmentation network training curves	47
4.5	Performance comparison of MSFusionXAI against established segmentation architectures. The proposed U-Net with ResNet34 encoder achieves a Dice score of 0.823, outperforming U-Net baseline (0.781), FCN-8s (0.745), and DeepLabv3+ (0. 792), while approaching the performance of Attention U-Net (0.805).	48

List of Figures

- 4.6 Attention weight analysis across 92 subjects showing modality preferences. **Left:** Scatter plot of learned attention weights with MRI attention (x-axis) vs clinical attention (y-axis). MS patients (red, n=46) cluster toward high MRI attention while healthy subjects (blue, n=46) show more balanced distributions. Dashed line indicates equal weighting (0.5, 0.5). **Right:** Box plots comparing attention distributions by modality and diagnosis, confirming statistically significant differences between groups. 49
- 4.7 Example BioBERT-generated automated diagnostic report for MS patient (Patient ID: MS-042). The structured report integrates classification results, attention weight analysis, lesion quantification, and clinical correlation into a comprehensive narrative suitable for electronic health record integration. Key sections include AI classification (95.4% MS probability), attention breakdown (82.4% MRI, 17.6% clinical), MRI findings (18 lesions, 12.7 mL total volume), and BioBERT-synthesized clinical impression emphasizing periventricular lesion distribution consistent with demyelinating disease. 51

List of Tables

1.1	Common Activation Functions in Artificial Neural Networks	14
1.2	Common types of XAI methods and their applications in medical AI.	19
2.1	Comprehensive comparison of multimodal MS detection and prediction studies. Key abbreviations: DSC=Dice-Sørensen Coefficient, PPV=Positive Predictive Value, AUC=Area Under the Curve, R ² =Coefficient of Determination, F1=F1-score.	26
2.2	Assessment of multimodal MS studies.	27
4.1	Classification performance across five cross-validation folds for MRI-only, Clinical-only, and Fusion models. Metrics include accuracy, precision, recall, and F1-score.	44
4.2	Average classification performance across five folds comparing MRI-only, Clinical-only, and Fusion approaches. Standard deviations quantify cross-fold variability.	44
4.3	Comparison of MSFusionXAI segmentation performance with state-of-the-art MS lesion segmentation methods. Dice coefficients, sensitivity, specificity, and architectural approaches are reported.	48

Acronyms

MS	<i>Multiple Sclerosis</i>
CNS	<i>Central Nervous System</i>
CSF	<i>Cerebrospinal Fluid</i>
OCB	<i>Oligoclonal Bands</i>
NfL	<i>Neurofilament Light Chain</i>
GFAP	<i>Glial Fibrillary Acidic Protein</i>
EDSS	<i>Expanded Disability Status Scale</i>
CIS	<i>Clinically Isolated Syndrome</i>
RRMS	<i>Relapsing-Remitting Multiple Sclerosis</i>
SPMS	<i>Secondary Progressive Multiple Sclerosis</i>
PPMS	<i>Primary Progressive Multiple Sclerosis</i>
MRI	<i>Magnetic Resonance Imaging</i>
FLAIR	<i>Fluid-Attenuated Inversion Recovery</i>
DTI	<i>Diffusion Tensor Imaging</i>
MTI	<i>Magnetization Transfer Imaging</i>
SWI	<i>Susceptibility-Weighted Imaging</i>
PET	<i>Positron Emission Tomography</i>
EEG	<i>Electroencephalography</i>

Acronyms

OCT	<i>Optical Coherence Tomography</i>
MRS	<i>Magnetic Resonance Spectroscopy</i>
CT	<i>Computed Tomography</i>
N4ITK	<i>N4 Bias Field Correction Tool (ITK Library)</i>
AI	<i>Artificial Intelligence</i>
ML	<i>Machine Learning</i>
DL	<i>Deep Learning</i>
XAI	<i>Explainable Artificial Intelligence</i>
MLP	<i>Multi-Layer Perceptron</i>
ANN	<i>Artificial Neural Network</i>
CNN	<i>Convolutional Neural Network</i>
RNN	<i>Recurrent Neural Network</i>
LSTM	<i>Long Short-Term Memory</i>
Bi-LSTM	<i>Bidirectional Long Short-Term Memory</i>
GRU	<i>Gated Recurrent Unit</i>
SVM	<i>Support Vector Machine</i>
RF	<i>Random Forest</i>
XGBoost	<i>Extreme Gradient Boosting</i>
GAN	<i>Generative Adversarial Network</i>
U-Net	<i>Convolutional Network Architecture for Image Segmentation</i>
ResNet	<i>Residual Neural Network</i>
DenseNet	<i>Densely Connected Convolutional Network</i>
BioBERT	<i>Bidirectional Encoder Representations from Transformers for Biomedical Text</i>

Acronyms

DNN	<i>Deep Neural Network</i>
QRIME	<i>Quantum RIME Metaheuristic</i>
AUC	<i>Area Under the Curve</i>
DSC	<i>Dice-Sørensen Coefficient</i>
PPV	<i>Positive Predictive Value</i>
R²	<i>Coefficient of Determination</i>
F1	<i>F1-Score</i>
NEDA	<i>No Evidence of Disease Activity</i>
ROC	<i>Receiver Operating Characteristic</i>
AUCROC	<i>Area Under ROC Curve</i>
TP	<i>True Positive</i>
FP	<i>False Positive</i>
FN	<i>False Negative</i>
TN	<i>True Negative</i>

General Introduction

Multiple Sclerosis (MS) is a serious, lifelong disease that affects the brain and spinal cord. It is caused by the body's own immune system attacking the protective covering of nerves, leading to inflammation, damage, and a slow loss of nerve function over time [1, 2]. The global impact of MS is large and continues to grow. Recent reports show that more than 2.9 million people around the world were living with MS in 2023 [80], with about 36 people in every 100,000 being affected [3]. This disease mainly strikes young adults between 20 and 50 years old. Women are affected nearly three times more often than men [4]. In many regions, especially where access to advanced medical care is limited, the burden of MS is even greater, leading to more disability [5].

Getting an accurate diagnosis of MS is difficult. The symptoms vary a lot from person to person and can look like other nerve diseases [6, 7]. Doctors usually follow the McDonald criteria, which combine results from brain scans (MRI), a clinical disability score (EDSS), and a test of spinal fluid (looking for oligoclonal bands) [6]. However, in everyday practice, these different pieces of information are often looked at separately. This **isolated approach** misses the full picture of how brain changes, physical disability, and biological markers are connected. It can delay diagnosis and make it harder to predict how the disease will progress. Also, the current method for measuring brain lesions on an MRI—drawing them by hand—is very slow and depends heavily on the expert doing it, leading to inconsistent results [8].

This is where Artificial Intelligence (AI) and Machine Learning can help. By combining different types of data—like MRI images, patient age, disability scores, and lab results—into smart computer models, we can improve how accurately and quickly MS is diagnosed. These models can find patterns that are hard for humans to see. However, a big problem stops these advanced AI tools from being used in hospitals: they often work like a *”black box.”** Doctors cannot see or understand how the AI made its decision, which makes it hard for them to trust the result [9]. For AI to be a helpful tool for neurologists, it must not only be accurate but also be able to **explain** its reasoning in a way that makes sense to a doctor.

This thesis tackles both of these problems—combining different data sources and making AI understandable—by introducing ****MSFusionXAI****. This is a new, explainable AI framework built to help detect and analyze Multiple Sclerosis. ****MSFusionXAI**** is based on three main ideas:

1. ****Accurate Lesion Measurement:**** A deep learning model (using a U-Net with a ResNet34 encoder) that automatically finds and outlines MS lesions on MRI scans, giving a precise and consistent measure of disease damage.
2. ****Smart Data Combination:**** A

General Introduction

new *adaptive attention* method that decides, for each patient, how much importance to give to the MRI images versus the clinical information (like age, sex, disability score, and spinal fluid results). This mimics how a doctor weighs different pieces of evidence.

3. **Clear Explanations:** A system that makes the AI's decision-making clear. It shows which type of data was most important, analyzes how lesion size relates to the diagnosis, and—critically—automatically writes a structured report in plain language using a medical AI (BioBERT), just like a doctor would.

We built and tested this system using real data from the CHU Sahloul University Hospital in Tunisia (46 MS patients and 46 healthy individuals). This work shows how to create a strong and useful AI tool even with the limited data often available in real hospitals. By focusing on explainability from the start, **MSFusionXAI** is designed to be a practical and trustworthy assistant for clinicians.

The main goals of this research are:

1. To build an efficient AI model that can automatically find MS lesions on MRI scans with a high level of accuracy, comparable to other advanced methods.
2. To create a new fusion technique that combines MRI and clinical data in a smart way, leading to better accuracy in telling MS patients apart from healthy people than using either type of data alone.
3. To build explainability directly into the system, using attention weights, statistical analysis, and automatic report writing, so that doctors can understand and trust the AI's conclusions.
4. To thoroughly test the entire **MSFusionXAI** system using a robust method called five-fold cross-validation, proving that it is more accurate and reliable than standard approaches, and showing it can fit into a hospital's workflow.

This thesis is organized as follows: **Chapter 1** explains the basics of MS and the key AI concepts used in this work. **Chapter 2** reviews recent research on using AI for MS diagnosis, highlighting the gaps that our framework aims to fill. **Chapter 3** describes the **MSFusionXAI** method in detail, from preparing the data to the design of each AI component. **Chapter 4** presents all the experiments and results, including tests of accuracy, speed, and explainability. Finally, **Chapter 5** summarizes what we have achieved, discusses the limitations, and suggests ideas for future improvements and real-world testing in clinics.

In summary, this thesis presents **MSFusionXAI**, a new tool that combines different types of medical data with clear, understandable AI to support the diagnosis of Multiple Sclerosis. By making the AI's reasoning transparent, we aim to build a tool that doctors can use with confidence to help their patients.

Chapter 1

Background Concepts

1.1 Introduction

Neurodegenerative disorders are caused by the progressive degeneration of cells and nervous system interconnections that are necessary for motion, balance, strength, sensation, and cognition. Multiple Sclerosis (MS) is a chronic and debilitating neurodegenerative condition that affects millions of individuals worldwide. It is characterized by demyelination and neuroinflammation within the central nervous system (CNS), which can result in motor dysfunction, sensory disturbances, and cognitive impairments. In this chapter, we present the medical and computer science foundations underpinning our proposed approach. The first section discusses the clinical and biological concepts of MS, while the second elaborates on the computational tools and artificial intelligence (AI) techniques relevant to MS detection and analysis.

1.2 Medical Concepts

1.2.1 Multiple Sclerosis (MS)

MS is a chronic inflammatory disorder of the CNS that primarily affects the brain and spinal cord. It results from an abnormal immune response targeting myelin, the protective sheath surrounding nerve fibers, leading to disrupted neural communication [10]. The disease manifests through episodes of demyelination followed by periods of remission, although it can progressively worsen over time. The exact etiology of MS remains unclear, but it is believed to involve a combination of genetic, environmental, and immunological factors [11]. Figure 1.1 illustrates the key pathological process comparing healthy myelinated nerves to MS-affected fibers.

At a cellular level, MS is characterized by the infiltration of autoreactive T cells into the CNS, triggering an inflammatory cascade that leads to myelin destruction and axonal damage [12]. This process is accompanied by gliosis and the formation of sclerotic plaques, which are hallmarks of MS observed in neuroimaging. Furthermore, recent research highlights the role of B cells in MS pathogenesis, emphasizing their contribution

to antibody-mediated responses and cytokine secretion [13].

Despite significant progress in understanding MS, it remains a highly heterogeneous disease with varying clinical presentations and progression patterns. The complexity of MS necessitates a multimodal approach for accurate diagnosis, incorporating neuroimaging, cerebrospinal fluid (CSF) biomarkers, and clinical evaluation [14].

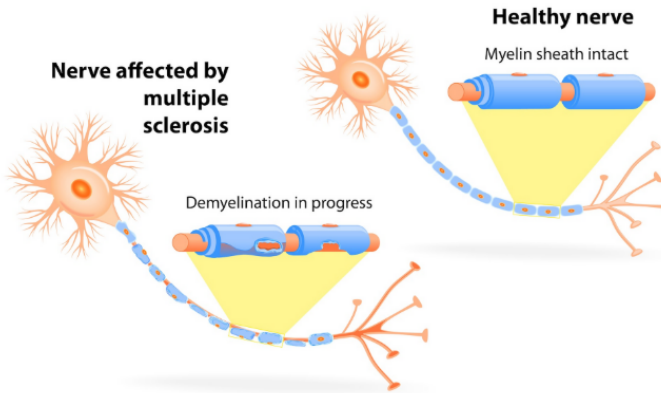


Figure 1.1: Neuropathological changes in MS [81].

1.2.2 Causes and Symptoms

MS arises from a complex interplay of genetic susceptibility and environmental triggers, leading to immune-mediated damage in the central nervous system. Genome-wide association studies (GWAS) have identified over 200 genetic variants linked to MS, particularly within the *HLA-DRB1* locus of the major histocompatibility complex (MHC) [15]. Individuals with a family history of MS have a higher risk, though heritability remains moderate compared to other autoimmune diseases [16]. Environmental factors also play a significant role; low vitamin D levels have been associated with increased susceptibility to MS due to their impact on immune regulation [17]. Epstein-Barr virus (EBV) infection is strongly correlated with MS onset, with recent studies suggesting it as a necessary trigger. Additionally, smoking has been linked to both increased MS risk and greater disease severity [18]. Geographic patterns indicate a higher prevalence in regions farther from the equator, suggesting an influence of sunlight exposure and vitamin D metabolism [19].

The early symptoms of MS vary but often include optic neuritis, presenting as blurred vision and pain with eye movement [20], sensory disturbances such as numbness and tingling [21], and profound fatigue [22]. Motor symptoms like limb weakness and spasticity are also common, affecting mobility [23]. A characteristic sign of MS is Lhermitte's phenomenon, described as an electric shock-like sensation traveling down the spine upon neck flexion, indicating cervical spinal cord involvement [24].

1.2.3 Stages of Multiple Sclerosis

Multiple Sclerosis (MS) progresses through distinct clinical subtypes, each exhibiting unique patterns of disease activity and disability accumulation (Figure 1.2). Understanding these stages is crucial for prognosis and treatment strategies [25].

1.2.3.1 Clinically Isolated Syndrome (CIS)

Clinically Isolated Syndrome (CIS) represents the first neurological episode suggestive of MS, lasting at least 24 hours. The diagnosis requires both clinical evidence of CNS demyelination and MRI findings consistent with MS, typically demonstrating two or more characteristic lesions. Approximately 60-80% of patients with CIS will develop clinically definite MS within two decades, with the risk significantly increased by the presence of gadolinium-enhancing lesions on MRI. Current evidence supports the use of disease-modifying therapies in high-risk CIS patients to delay conversion to MS [26].

1.2.3.2 Relapsing-Remitting MS (RRMS)

RRMS is the most common form, affecting approximately 85% of MS patients at diagnosis. It is characterized by episodic relapses—new or worsening neurological symptoms—followed by periods of partial or complete remission. MRI findings typically show inflammatory demyelinating lesions, with gadolinium-enhancing areas indicating active disease [27].

1.2.3.3 Secondary Progressive MS (SPMS)

SPMS usually develops after a period of RRMS, with a transition marked by gradual worsening of neurological function, independent of discrete relapses. This stage is associated with increased neurodegeneration, brain atrophy, and axonal loss, which contribute to accumulating disability over time. While inflammation persists, it plays a reduced role compared to earlier stages [28].

1.2.3.4 Primary Progressive MS (PPMS)

PPMS accounts for about 10–15% of cases and is characterized by continuous symptom progression from onset, without clear relapses or remissions [29]. Unlike RRMS, PPMS exhibits fewer inflammatory lesions but greater spinal cord involvement, leading to significant motor impairment. Patients with PPMS often experience a more aggressive disability trajectory, with fewer treatment options available, though recent therapies targeting B cells have shown promise [30].

These MS subtypes highlight the complexity of disease progression, emphasizing the need for personalized treatment approaches and continued research into disease-modifying therapies.

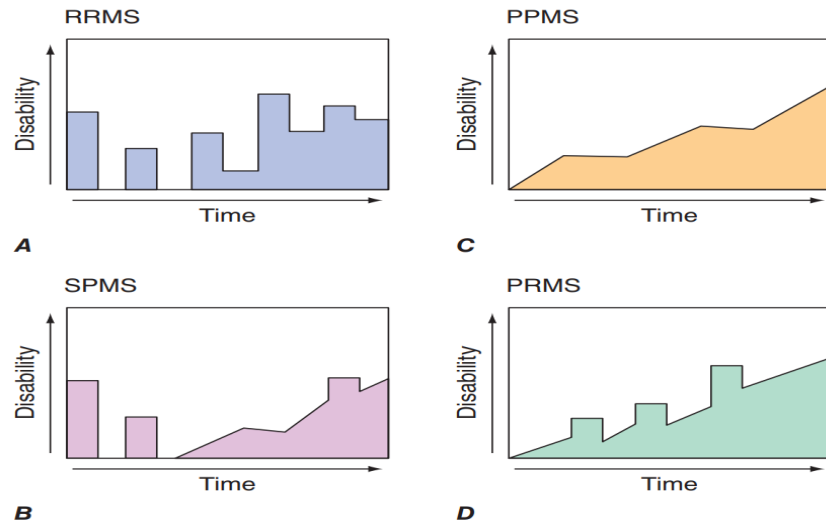


Figure 1.2: Multiple sclerosis subtypes [30]..

1.2.4 MS Detection Methods

Accurate diagnosis of Multiple Sclerosis (MS) relies on a combination of clinical evaluation, magnetic resonance imaging (MRI), cerebrospinal fluid (CSF) analysis, and established diagnostic criteria.

1.2.4.1 MRI in MS Detection

Magnetic Resonance Imaging (MRI) is the gold standard imaging technique for diagnosing and monitoring Multiple Sclerosis (MS) [8, 6]. Its importance stems from several key advantages:

- **Early and Accurate Diagnosis:** MRI can detect MS lesions in the brain and spinal cord even before clinical symptoms appear, allowing for earlier diagnosis and intervention [6].
- **Objective Visualization of Lesions:** MRI provides high-resolution, detailed images that reveal the size, number, and location of demyelinating lesions, particularly in regions characteristic for MS such as periventricular, juxtacortical, infratentorial, and spinal cord areas [31].
- **Assessment of Disease Activity:** By comparing new scans with previous ones, clinicians can identify new or enlarging lesions and differentiate between active (gadolinium-enhancing) and chronic lesions. This helps guide treatment decisions and monitor therapeutic response [8].
- **Support for Diagnostic Criteria:** The McDonald criteria for MS diagnosis rely heavily on MRI to demonstrate both dissemination in space (multiple regions affected) and dissemination in time (lesions appearing at different times), increasing diagnostic confidence and reducing the need for invasive procedures [6].

- **Research and Innovation:** MRI data are essential for computational analysis, including automated lesion detection and segmentation, and serve as a foundation for artificial intelligence applications in MS research [32, 33].

1. **MRI Sequences in MS** MRI scans are acquired using different imaging sequences, each optimized to highlight specific tissue characteristics. The most commonly used sequences in MS detection include:

- **T1-weighted (T1-w) images:** Provide high-resolution anatomical details. When combined with gadolinium contrast agents, T1-w scans help detect active lesions by identifying areas with a compromised blood-brain barrier [34].
- **T2-weighted (T2-w) images:** Sensitive to water content and inflammation, these images are effective in detecting the total burden of MS lesions. Hyperintense regions on T2-w images typically correspond to demyelinated plaques [35].
- **Fluid-Attenuated Inversion Recovery (FLAIR):** Suppresses cerebrospinal fluid (CSF) signals, enhancing the visibility of periventricular and juxtacortical lesions that are characteristic of MS [31].
- **Advanced MRI Techniques:** These include diffusion tensor imaging (DTI), magnetization transfer imaging (MTI), and susceptibility-weighted imaging (SWI), which provide insights into microstructural damage and chronic lesions [36, 37].

2. **2D vs. 3D MRI in MS** MRI data can be acquired as either two-dimensional (2D) slices or three-dimensional (3D) volumes. **3D MRI has gained prominence in MS research** due to its isotropic resolution and suitability for AI-based segmentation tasks (e.g., 3D U-Net models) [33, 32]. Spinal cord imaging, though technically challenging, is critical for comprehensive MS assessment [38].

The characteristic distribution of lesions—periventricular, juxtacortical, infratentorial, and spinal cord—is a key diagnostic criterion in MS, as outlined by the McDonald criteria [6].

The ability of MRI to combine sensitivity, specificity, and detailed visualization of MS pathology makes it indispensable in clinical practice and research.

1.2.4.2 CT Imaging in MS Detection

Computed Tomography (CT) is not a primary imaging modality for diagnosing multiple sclerosis (MS) due to its limited sensitivity for detecting white matter lesions and inferior soft tissue contrast compared to MRI. However, CT can play a supplementary role in specific scenarios, such as detecting gross structural changes like brain atrophy in progressive MS or ruling out alternative diagnoses (e.g., brain tumors, acute stroke, or hemorrhage) when MRI is unavailable or contraindicated[39]. For instance, CT may identify cortical atrophy, which correlates with disability progression in advanced MS cases, though it lacks the resolution to visualize early demyelinating lesions[40]. Recent

consensus guidelines and neuroimaging reviews emphasize MRI as the gold standard and do not recommend CT for routine MS diagnosis or monitoring, limiting its use to acute or resource-constrained settings[39, 40].

1.2.4.3 CSF Biomarkers in Multiple Sclerosis

Cerebrospinal fluid (CSF) analysis is an important diagnostic tool for multiple sclerosis (MS) as it detects inflammation and nerve damage in the central nervous system. The main CSF biomarkers are:

- **Oligoclonal Bands (OCBs):** OCBs are present in the vast majority of MS patients and strongly support the diagnosis when combined with MRI findings, though they are not unique to MS [14].
- **Neurofilament Light Chain (NfL):** Higher CSF NfL levels indicate nerve fiber damage and correlate with disease activity and progression [41].
- **Emerging Biomarkers:** Additional biomarkers such as chitinase-3-like-1 (CHI3L1) and glial fibrillary acidic protein (GFAP) are under investigation for their potential to track MS subtypes and progression.

1.2.4.4 Clinical History and Diagnostic Criteria

Diagnosing MS combines clinical assessment, neurological examination, and paraclinical tests. The McDonald criteria [6] are widely used and focus on:

- **Dissemination in space:** Lesions in different regions of the central nervous system, identified by MRI.
- **Dissemination in time:** Evidence that lesions have developed at different points in time, shown on MRI or by new clinical symptoms. OCBs can substitute for this in some cases.

Early symptoms that may suggest MS include vision problems (optic neuritis), abnormal sensations (numbness, tingling), muscle weakness or stiffness, and occasionally balance or double vision [20, 23].

It is essential to rule out other conditions that can mimic MS, such as neuromyelitis optica, vitamin B12 deficiency, and certain infections [42].

1.2.5 Limitations of MS Detection Methods

Despite advancements, current MS diagnostic methods have inherent limitations. MRI findings, though crucial for diagnosis, are not exclusive to MS, as similar lesions can appear in conditions like neuromyelitis optica spectrum disorders and small vessel ischemic disease, leading to potential misdiagnosis [42]. Additionally, MRI may not detect early microscopic changes, necessitating complementary diagnostic tools [31].

Similarly, CT scans are limited by their low sensitivity for MS-specific lesions and the use of ionizing radiation, restricting their application to specific diagnostic scenarios [39].

CSF biomarkers, such as oligoclonal bands (OCBs) and neurofilament light chain (NfL), while useful, lack disease specificity, as they can also be elevated in other neurological disorders [43, 41]. Clinical diagnosis based on the McDonald criteria, though widely adopted, may produce false positives, particularly when MRI findings are nonspecific or when early MS symptoms overlap with other neurological conditions [44, 45].

These limitations highlight the need for more integrative and intelligent diagnostic solutions. The complexity of MS—ranging from its clinical heterogeneity to its subtle radiological signatures—requires systems capable of synthesizing diverse data types. Artificial Intelligence (AI), particularly when applied in multimodal frameworks, holds the potential to overcome many of these diagnostic shortcomings. By combining imaging, clinical, and biological information, AI-powered models can enhance diagnostic precision, uncover latent patterns, and support early intervention.

1.3 Computer Science Concepts

Computer science plays a central role in advancing Multiple Sclerosis (MS) research by applying artificial intelligence to analyze MRI scans, clinical records, and CSF biomarkers. Through preprocessing, feature extraction, data integration, and explainable AI, these methods support accurate diagnosis and better understanding of disease progression.

1.3.1 Data Preprocessing

1.3.1.1 Medical Image Preprocessing

Medical image preprocessing is a set of techniques to standardize MRI scans by removing artifacts and enhancing key features for accurate multiple sclerosis (MS) analysis. It ensures clear visualization of brain structures, such as lesions, by correcting noise and distortions. This enables consistent image comparison across patients and timepoints, forming a critical foundation for MS research and diagnosis [46].

1. Bias Field Correction :

MRI scans may have smooth intensity variations caused by magnetic field imperfections. This effect, called a bias field, makes similar tissues look different in brightness. Bias field correction solves this problem and makes the image clearer and more uniform. The most commonly used method is N4ITK, which improves tissue visibility and supports better model performance [47].

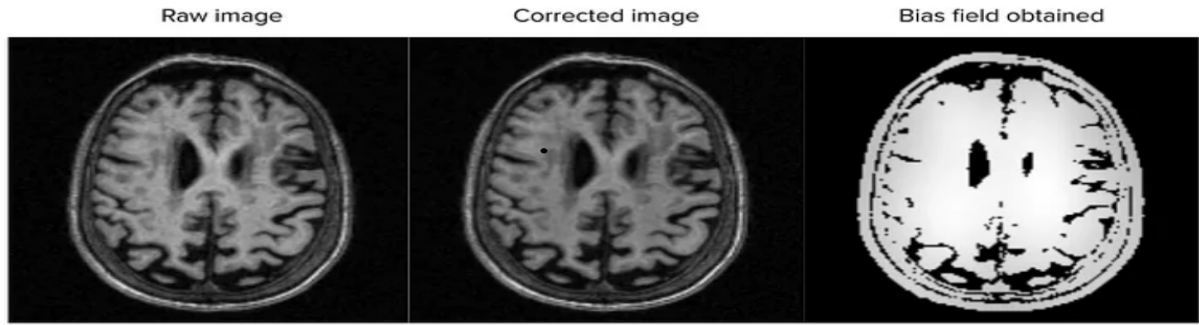


Figure 1.3: Raw MRI image (left) with visible bias field; corrected image (right) using N4ITK [82].

2. Skull Stripping :

Skull stripping is the process of removing non-brain parts such as the skull and scalp from MRI images. This step helps focus only on the brain regions, especially white matter where MS lesions usually appear. It also makes the processing faster and more accurate. Tools like BET (Brain Extraction Tool) or ROBEX are commonly used for this task [48].

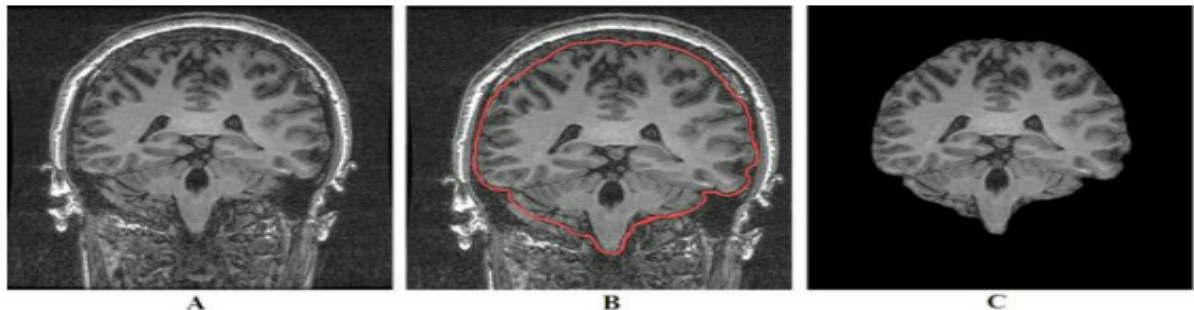


Figure 1.4: Skull-stripping steps in MRI preprocessing: (A) Original input image, (B) Brain tissue contouring, and (C) Removal of non-brain tissues [49].

3. Resampling :

MRI scans from different machines may have different resolutions. Resampling adjusts all images to the same voxel size (e.g., $1 \times 1 \times 1 \text{ mm}^3$). This helps ensure that models analyze images in a consistent way, especially when combining data from different hospitals or studies [50].

4. Denoising :

MRI scans often contain noise due to scanner limitations or patient movement. Denoising techniques help reduce this noise while preserving important features like edges and lesions. One popular method is the Non-Local Means (NLM) filter, which smooths the image by comparing patches with similar intensity patterns [51]. Figure 1.5 illustrates the impact of denoising, comparing a raw MRI scan with its processed counterpart.

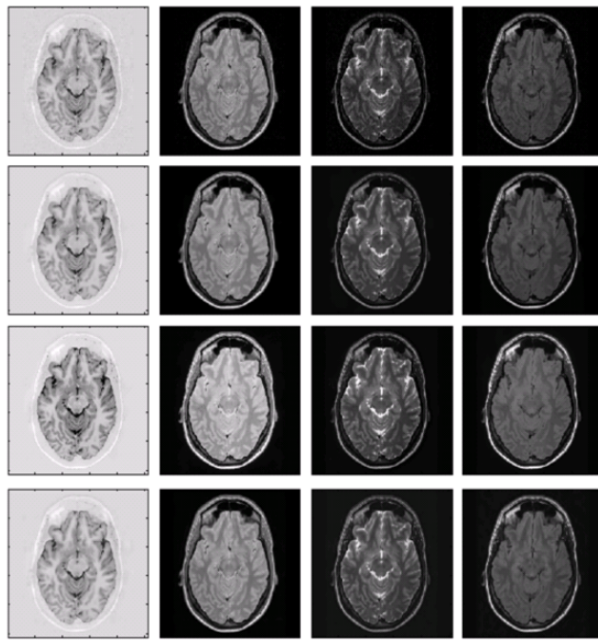


Figure 1.5: Denoising results: (Top) Original noisy MRI, (Bottom) Denoised output [51].

5. Intensity Normalization :

MRI brightness variations caused by scanner differences are standardized through intensity normalization, ensuring biologically relevant contrasts [52]. Figure 1.6 shows the transformation from raw to normalized images using histogram alignment. Methods like IAMLAB and WhiteStripe excel at preserving FLAIR pathology while removing technical variability [53].

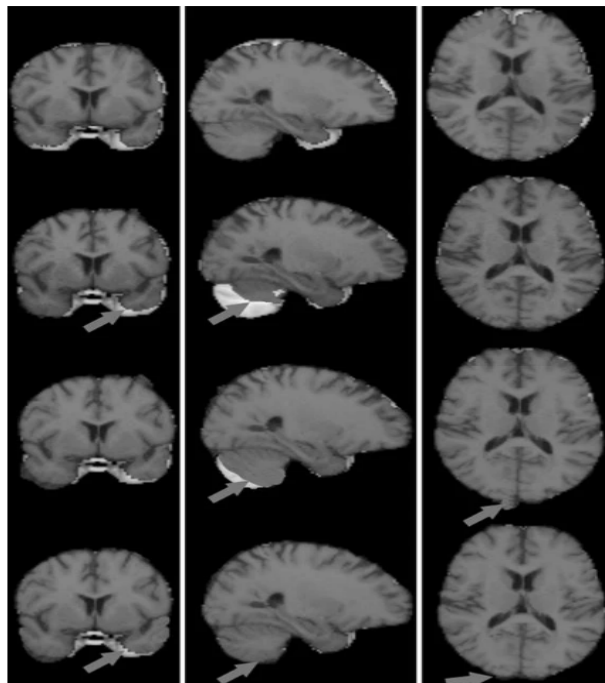


Figure 1.6: Intensity normalization stages: Reference (top), input, histogram-matched, and WhiteStripe-normalized results [53].

1.3.1.2 Text and Clinical Data Preprocessing

Preprocessing of clinical data involves preparing structured data (e.g., clinical history, biomarkers) and unstructured data (e.g., clinical notes) for multiple sclerosis (MS) research. This ensures data quality and compatibility with computational models, addressing irregularities to enable insights into disease progression. Examples include clinical history (age, sex, EDSS) and cerebrospinal fluid (CSF) biomarkers (neurofilament light chain (NfL), oligoclonal bands (OCB)) [54].

1. **Data Cleansing :** Data cleansing corrects errors, removes duplicates, resolves inconsistencies, and handles missing values. For structured data, such as clinical history or biomarkers, this may involve imputing missing entries (e.g., EDSS scores or NfL levels).
2. **Normalization of Clinical Variables :** Normalization adjusts numerical data to a common scale (e.g., [0,1]) to prevent variables with larger ranges from dominating analyses. This applies to data like age, clinical scores (e.g., EDSS), or biomarker levels (e.g., NfL), ensuring equitable contribution and improving model performance in MS research.
3. **Categorical Variable Encoding :** Categorical variables (e.g., sex, OCB status) are converted into a numerical format suitable for machine learning models. Common techniques include label encoding (assigning an integer to each category) or one-hot encoding (creating binary columns for each category).

1.3.2 Artificial Intelligence

Artificial Intelligence (AI) is a core area of computer science focused on creating systems capable of performing tasks that typically require human intelligence. These tasks include reasoning, learning, problem-solving, perception, and natural language understanding. Within the landscape of computer science, AI provides the theoretical and algorithmic foundation for a wide array of applications, ranging from data analysis to autonomous systems. In the context of healthcare and beyond, AI serves as a powerful tool for extracting insights from complex, high-dimensional datasets, enabling data-driven decision support across domains [55, 56].

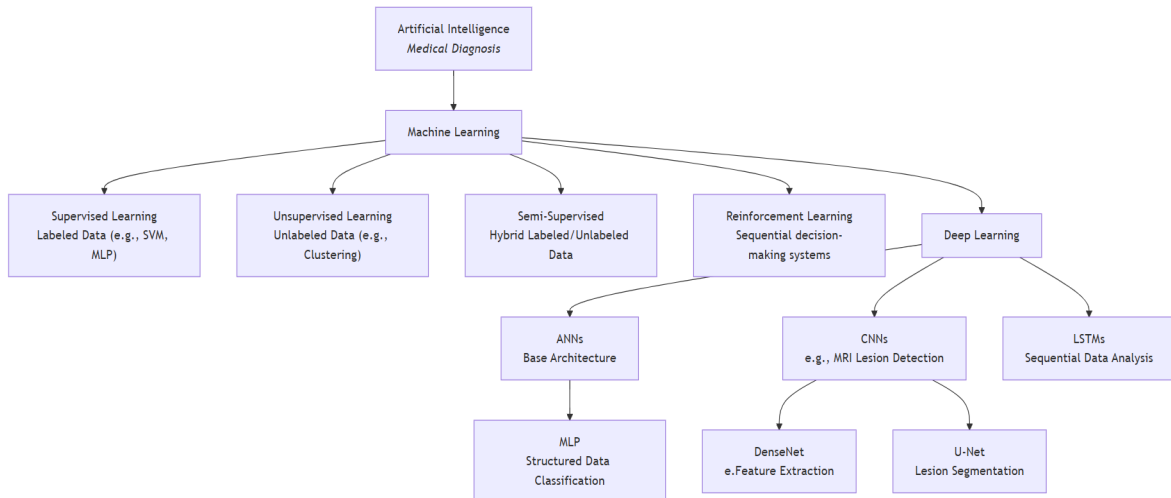


Figure 1.7: Hierarchical overview of Artificial Intelligence techniques in Medical Diagnosis.

1.3.2.1 Machine Learning (ML)

Machine learning (ML), a core subfield of AI, develops algorithms capable of learning from data without being explicitly programmed. It is particularly effective in modeling structured clinical data such as patient demographics, lab values, and diagnostic scores. Common ML models include Support Vector Machines (SVMs), Random Forests, and Multi-Layer Perceptrons (MLPs), all of which are used for pattern recognition, anomaly detection, and classification tasks [57]. ML approaches include:

- **Supervised Learning:** Models are trained using labeled data (e.g., images tagged with diagnoses), enabling tasks such as disease detection or treatment outcome prediction.
- **Unsupervised Learning:** Patterns are extracted from unlabeled data through techniques like clustering, useful for discovering hidden subgroups or phenotypes in a patient population.
- **Semi-Supervised Learning:** Combines a small set of labeled data with a larger pool of unlabeled data to improve model generalization when annotations are scarce.
- **Reinforcement Learning:** Uses trial-and-error strategies to make sequential decisions, optimizing processes such as treatment planning or adaptive diagnostics.

1.3.2.2 Artificial Neural Networks (ANNs)

Artificial Neural Networks (ANNs) are computational models inspired by biological neural networks, consisting of interconnected processing units called neurons. As shown in Figure 1.8, a typical ANN architecture includes:

- An **input layer** that receives raw data

- One or more **hidden layers** that transform inputs through learned patterns
- An **output layer** that produces final predictions

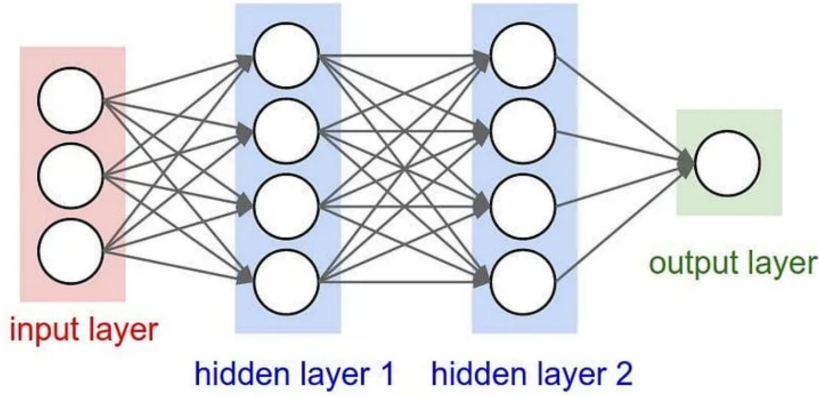


Figure 1.8: Architecture of a fully-connected neural network showing input, hidden, and output layers with weighted connections between neurons.

Each neuron processes information in two stages:

1. Computes a weighted sum: $z = \mathbf{w}^T \mathbf{x} + b$
2. Applies an activation function: $a = f(z)$

These activation functions introduce essential non-linearities that enable ANNs to approximate complex functions. Table 1.1 summarizes the most common activation functions and their properties:

Table 1.1: Common Activation Functions in Artificial Neural Networks

Function	Mathematical Formula	Properties and Applications
Sigmoid	$\sigma(x) = \frac{1}{1+e^{-x}}$	Range: (0, 1); smooth gradient; suffers from vanishing gradients; used in binary classification output layers.
Hyperbolic Tangent (Tanh)	$\tanh(x) = \frac{e^x - e^{-x}}{e^x + e^{-x}}$	Range: (-1, 1); zero-centered output; stronger gradients than sigmoid; used in hidden layers.
Rectified Linear Unit (ReLU)	$\text{ReLU}(x) = \max(0, x)$	Range: [0, ∞); computationally efficient; avoids vanishing gradient for positive inputs; may cause “dead neurons”; default choice for hidden layers.
Leaky ReLU	$\text{LReLU}(x) = \begin{cases} x, & x \geq 0 \\ 0.01x, & x < 0 \end{cases}$	Range: $(-\infty, \infty)$; prevents dead neurons; small negative slope (typically $\alpha = 0.01$); used when ReLU causes too many inactive neurons.
Softmax	$\text{Softmax}(x_i) = \frac{e^{x_i}}{\sum_{j=1}^n e^{x_j}}$	Outputs probability distribution (sums to 1); used exclusively in output layers; for multi-class classification; generalization of sigmoid for multiple classes.

1.3.2.3 Deep Learning (DL)

Deep Learning (DL) is an advanced branch of ML that uses multi-layered neural networks to learn hierarchical representations of data. DL is especially effective in analyzing large-scale, high-dimensional inputs such as radiological images, histopathology slides, or textual clinical notes. By automatically learning features through its layered architecture, DL enables nuanced data interpretation without the need for manual feature engineering [58].

1.3.2.4 Convolutional Neural Networks (CNNs)

CNNs are designed to process grid-like data such as images. Their architecture is composed of several distinct layers that operate in sequence to extract and process features from input data [59]:

- **Convolutional Layer:** Applies a set of learnable filters (kernels) to the input, producing feature maps that capture spatial hierarchies.
- **Activation Layer:** Introduces non-linearity into the model, typically using the ReLU (Rectified Linear Unit) function.
- **Pooling Layer:** Reduces the spatial dimensions of the feature maps, retaining the most important information and providing translation invariance (commonly max pooling or average pooling).
- **Fully Connected (FC) Layer:** Each neuron in this layer is connected to all neurons in the previous layer. FC layers are generally used at the end of the network to perform classification based on the extracted features.

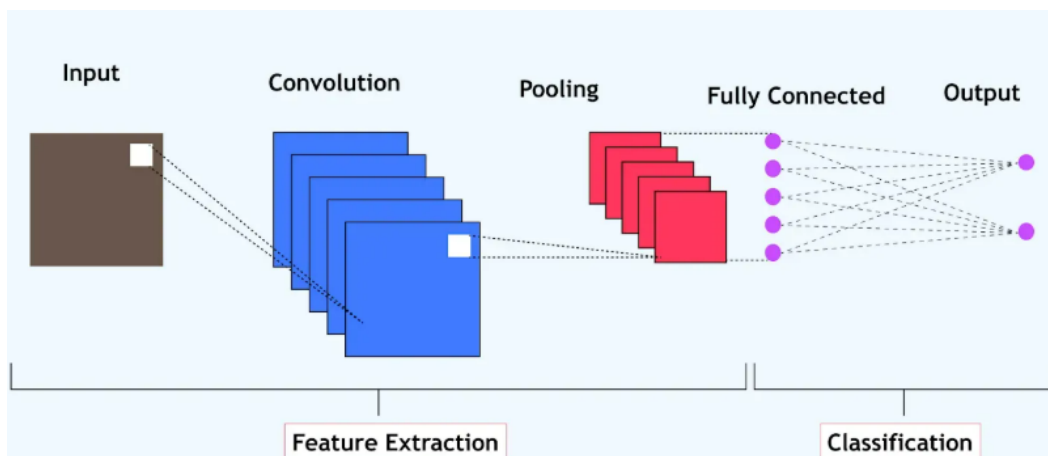


Figure 1.9: Typical architecture of a Convolutional Neural Network (CNN) showing convolution, activation, pooling, and fully connected layers[83].

1.3.2.5 DenseNet

DenseNet architectures feature dense connections between layers, meaning each layer receives inputs from all preceding layers. This connectivity pattern improves information and gradient flow throughout the network, which can lead to more accurate and efficient models [60].

- **Dense Connectivity Principle :**

In DenseNet, each layer receives inputs from all preceding layers, allowing efficient information flow, better gradient propagation, and extensive feature reuse.

- **Dense Block and Transition Layers :**

A dense block is a group of layers with this dense connectivity. Transition layers, placed between dense blocks, use batch normalization, 1 convolutions, and 2 pooling to reduce feature map size and control model complexity.

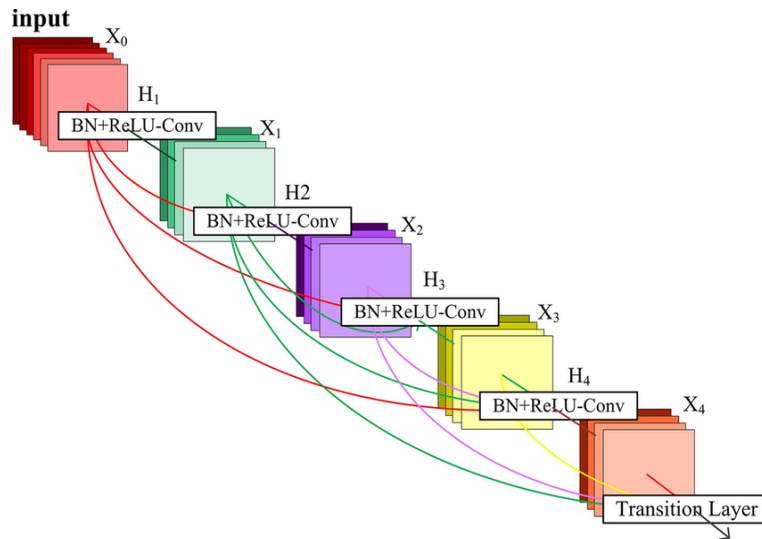


Figure 1.10: DenseNet block illustration: each layer receives input from all previous layers, followed by a transition layer [61].

1.3.2.6 U-Net

U-Net is a convolutional network architecture for fast and precise image segmentation, especially in biomedical imaging [32].

- **Encoder-Decoder Structure :**

U-Net consists of two paths:

- **Encoder (Contracting path):** This path captures context in the image through repeated application of convolutional and pooling layers, progressively reducing the spatial dimensions while increasing feature depth.
- **Decoder (Expanding path):** This path performs upsampling and convolution to reconstruct the spatial dimensions, enabling precise localization of features.

- Skip Connections :

Skip connections directly link corresponding layers in the encoder and decoder paths. These connections concatenate feature maps from the encoder to the decoder, preserving spatial information lost during downsampling and aiding in more accurate segmentation.

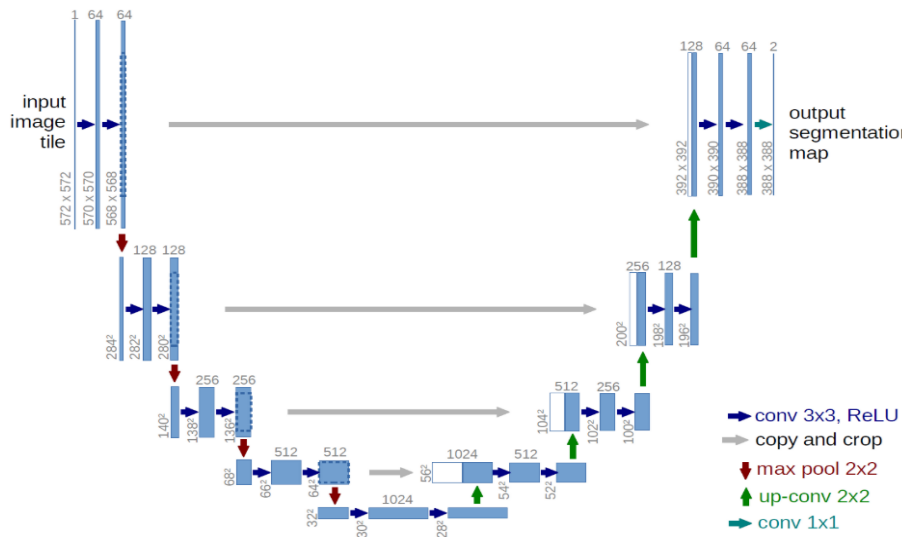


Figure 1.11: U-Net architecture: encoder-decoder structure with skip connections, showing convolution, pooling, up-convolution, and output segmentation map [32].

1.3.2.7 ResNet34

ResNet34 is a residual neural network architecture composed of 34 layers, designed to mitigate the vanishing gradient problem through the use of residual connections. These skip connections allow the network to learn identity mappings, improving gradient flow and enabling the training of deeper networks [62].

- **Residual Connections:**

In ResNet34, each residual block adds the input of the block to its output via a shortcut connection. This facilitates learning of residual functions rather than direct mappings, improving convergence and overall performance.

- Residual Blocks and Downsampling:

A residual block typically contains two or three convolutional layers with batch normalization and ReLU activations. Downsampling is performed using convolutional layers with stride 2 at certain blocks, reducing feature map size while increasing receptive field.

1.3.2.8 Multi-Layer Perceptron (MLP)

A Multi-Layer Perceptron (MLP) is a basic form of ANN where data moves unidirectionally from input to output through one or more hidden layers. MLPs are primarily used

for tasks involving structured data, such as patient records, sensor readings, or tabulated test results. Their ability to model complex, non-linear relationships makes them suitable for classification and regression tasks in clinical decision support [54].

1.3.2.9 Long Short-Term Memory Networks (LSTM)

Long Short-Term Memory (LSTM) networks are a type of recurrent neural network (RNN) capable of learning long-term dependencies in sequential data. They are especially useful in analyzing time-series health data such as vital sign trends, symptom progression, or treatment response over time. LSTMs maintain internal memory states, allowing them to make informed predictions based on historical input sequences [58].

1.3.3 Data Integration

Data integration is a comprehensive process in MS research that involves combining multiple types of data—such as MRI scans, CSF biomarkers, and clinical records—into a single, cohesive representation to enhance the overall analysis of the disease. This approach recognizes the complementary nature of different data sources, each providing unique perspectives on MS, and seeks to unify them to create a more complete picture of the condition [58].

- **Feature Alignment:**

Feature alignment is the initial step in data integration, where features extracted from various data sources are adjusted to ensure they share a consistent dimensionality and semantic meaning. This harmonization allows for a unified analysis by aligning the diverse characteristics of MS data, such as imaging features and clinical measurements, into a compatible format.

- **Attention-Based Fusion:**

Attention-based fusion is a dynamic technique within data integration that assigns varying levels of importance to different data types based on their relevance to the analysis. This method enables the system to focus on the most pertinent information—such as imaging data for lesion detection or clinical data for assessing progression—ensuring a balanced and context-sensitive integration process.

- **Fused Representation:**

Fused representation is the resulting unified data structure that encapsulates the integrated features from multiple sources, serving as a foundation for further analytical tasks. This combined representation provides a holistic view of MS, consolidating the strengths of each data type to support comprehensive diagnostic or research efforts.

1.3.4 Explainable Artificial Intelligence (XAI)

Explainable Artificial Intelligence (XAI) aims to make the decision-making processes of complex models transparent and understandable, which is crucial in MS research where

diagnostic accuracy and trust are essential. By clarifying how predictions are generated, XAI addresses the "black box" problem of advanced models, ensuring their outputs can be interpreted and validated by clinicians and researchers [63]. The main types of XAI methods commonly used in medical AI are summarized in Table 1.2.

1.3.4.1 Attention-Based Explanation

Attention-based explanation uses attention mechanisms to highlight the relative contribution of different input elements to a model's output. In MS research, this approach can reveal which imaging features or clinical observations most influence a prediction, offering visual or quantitative insights that support clinical decision-making [64].

1.3.4.2 Natural Language Explanation

Natural language explanation generates human-readable descriptions from model outputs, often using generative language models. In MS research, this technique can provide textual summaries, such as indicating that a prediction relies on specific imaging patterns, making the model's reasoning accessible to clinicians and supporting the integration of AI tools into practice [63].

Table 1.2: Common types of XAI methods and their applications in medical AI.

Method	Description	Example Usage
Attention-Based	Highlights important features/modalities	Which input influenced the prediction most
Saliency/Grad-CAM	Visual heatmap over input features (e.g., MRI regions)	Shows relevant image regions
Feature Importance	Quantifies contribution of each feature	Ranks clinical variables by influence
Natural Language	Generates textual explanation	Summarizes reasoning in plain language
Post-hoc (LIME, SHAP)	Model-agnostic local explanations	Explains individual predictions

1.4 Conclusion

This chapter has established a solid foundation by defining key computer science concepts essential for MS research, including preprocessing, AI architectures, data integration, and explainability. These concepts provide a broad understanding of computational tools that support MS analysis, setting the stage for deeper exploration in subsequent chapters. This groundwork will guide the development of tailored methodologies to advance MS diagnosis and treatment strategies.

Chapter 2

State-Of-The-Art in Multimodal MS Detection

2.1 Introduction

Traditional MS detection methods, such as MRI, CSF biomarkers, and clinical evaluations, have limitations in accuracy and early diagnosis. Multimodal approaches aim to improve detection by integrating multiple data sources, leveraging AI and deep learning for enhanced analysis. These methods not only boost diagnostic precision but also provide explainability, aiding clinical decision-making. This chapter reviews recent multimodal techniques for MS detection, comparing their effectiveness and challenges. A summary table highlights key findings, followed by a discussion on future research directions.

2.1.1 Multimodal Data in MS Detection

The integration of diverse data modalities offers a holistic view of multiple sclerosis (MS), capturing its multifaceted pathology and enhancing diagnostic accuracy. Multimodal strategies leverage the complementary strengths of imaging, clinical assessments, and molecular biomarkers to overcome the limitations inherent in any single modality. This multimodal perspective is essential because MS manifests through structural brain changes, clinical symptoms, and immunological abnormalities that are not all visible on a single test. :contentReference[oaicite:0]index=0

2.1.1.1 Imaging Modalities

Magnetic resonance imaging (MRI) remains the cornerstone of MS diagnosis and monitoring owing to its sensitivity to demyelinating lesions and neurodegeneration. Standard sequences used in clinical and research practice include T1-weighted (for anatomy and “black holes”), T2-weighted (for total lesion burden), and FLAIR (which suppresses CSF and enhances periventricular/juxtacortical lesion visibility). Advanced sequences such as diffusion tensor imaging (DTI), magnetization transfer imaging (MTI) and susceptibility-weighted imaging (SWI) add microstructural and tissue-integrity information that com-

plements conventional contrasts.

Large multicentre cohorts and consortia have demonstrated the value of combining MRI with other modalities: for example, the FutureMS cohort (Kearns et al., 2022) integrates MRI with genetic and biomarker data to enable individualized prediction models in newly diagnosed RRMS patients. Multimodal imaging studies have also explored PET markers of neuroinflammation and EEG measures of functional connectivity as complementary sources of pathophysiological information, particularly when studying progression or conversion to secondary progressive MS. These alternative modalities are promising for specific research questions (neuroinflammation, metabolism, connectivity) but remain largely adjunctive to MRI in routine diagnosis.

Practical considerations — such as 2D vs 3D acquisitions, spinal cord imaging challenges, and harmonization across scanners — strongly influence the choice of sequences for AI-driven analyses. The literature favors 3D, isotropic acquisitions when possible for volumetric and deep-learning segmentation tasks, while also recognizing that spinal cord imaging has specific technical constraints that require bespoke preprocessing and acquisition protocols. :contentReference[oaicite:3]index=3

2.1.1.2 Clinical Assessments and Health Records

Clinical variables (e.g., Expanded Disability Status Scale — EDSS — scores, neurological exam findings, symptom history, cognitive test results) provide indispensable context for image-based findings. These measures capture functional impact and temporal disease dynamics that MRI alone may not reflect. Several studies demonstrate that integrating structured clinical data or EHR-derived features with imaging significantly improves predictive performance and clinical relevance. For instance, Ismail et al. (2024) reported near-perfect classification accuracy when combining MRI-derived deep features with electronic health records in a multimodal pipeline, illustrating the strong synergy between image and clinical sources. Integrating longitudinal clinical records also enables temporal modelling of disease activity and better risk stratification.

However, variability and missingness in clinical records (different scoring habits, intermittent documentation) present challenges for multimodal pipelines. Real-world integration therefore typically requires rigorous preprocessing (imputation, normalization, encoding), temporal alignment, and attention to bias introduced by heterogeneous documentation standards. :contentReference[oaicite:5]index=5

2.1.1.3 Biofluid Biomarkers

Biofluid markers from cerebrospinal fluid (CSF) and blood provide molecular-level evidence of inflammation and neuroaxonal injury that complements MRI and clinical assessments. Classical CSF markers such as oligoclonal bands (OCBs) and κ -free light chains remain clinically useful for diagnosis and can substitute for dissemination-in-time in some contexts. Blood biomarkers, particularly serum neurofilament light (sNfL) and GFAP, are increasingly used as minimally invasive indicators of active axonal damage and disease progression. Several recent reviews and cohort studies report that combining sNfL/GFAP

with MRI metrics (and cognitive scores) improves prognostic models for disability and cognitive decline.

Limitations of biofluid markers include imperfect disease specificity (values may be elevated in other neurological disorders) and variability across assay platforms. Nevertheless, the consensus in multimodal studies is that biomarkers markedly increase confidence in early or ambiguous cases when combined with imaging and clinical measures.

2.1.1.4 Multimodal Data Integration and Artificial Intelligence

The heterogeneity, high dimensionality, and modality-specific noise of multimodal MS data motivate the use of AI and data-fusion frameworks. Deep learning and hybrid architectures enable automatic representation learning from images while classical and modern ML methods can ingest tabular clinical/biomarker data; fusion strategies (early, late, hybrid, attention-based) reconcile these sources in a coherent model. Reviews in the field underline that AI-driven multimodal fusion can address missing data, heterogeneous acquisition protocols, and cross-site variability, producing models that better capture phenotypic heterogeneity and improve clinical tasks such as diagnosis, prognosis, and patient stratification.

In practice, multimodal integration must be paired with careful preprocessing (harmonization, normalization), robust validation across cohorts, and techniques to mitigate modality-dominance (i.e., when one modality consistently outweighs others in model decisions). Attention-based fusion and modular pipelines are commonly proposed solutions in recent literature. :contentReference[oaicite:9]index=9

2.1.2 Machine Learning and Deep Learning in Multimodal MS Analysis

Machine learning (ML) and deep learning (DL) have become central to modern MS research because they can integrate heterogeneous data sources—MRI, clinical variables, cognitive scores, and cerebrospinal fluid (CSF) biomarkers—into unified predictive models. Traditional diagnostic workflows rely on expert interpretation of MRI alongside clinical criteria such as the 2017 McDonald guidelines, yet ML/DL systems enable systematic extraction of subtle imaging patterns, quantitative lesion metrics, and non-linear interactions between biological and clinical indicators. Recent reviews emphasize that multimodal AI systems significantly outperform single-modality pipelines by capturing complementary information from structural injury, inflammatory activity, and patient-specific disease trajectories [2].

2.1.2.1 Deep Learning for Multimodal Feature Representation

Deep learning has driven most breakthroughs in multimodal MS analysis due to its ability to learn hierarchical representations from imaging while simultaneously encoding structured tabular variables. Convolutional neural networks (CNNs)—including ResNet, DenseNet, and U-Net-based encoders—are widely employed to extract high-level MRI fea-

tures such as lesion morphology, periventricular distribution, cortical involvement, and microstructural abnormalities. These representations can be fused with vectors representing EDSS scores, OCB status, demographic information, and additional clinical variables. Multimodal studies consistently report major gains when combining CNN-derived MRI features with clinical or EHR data, often improving AUROC by 8–15% compared to single-modality setups [54, 58].

Hybrid deep learning architectures typically rely on modality-specific encoders followed by shared fusion layers. For instance, models using DenseNet or ResNet for MRI feature extraction and multilayer perceptrons (MLPs) or recurrent units for clinical time-series data have demonstrated improved prediction of disease activity, conversion from CIS to MS, and cognitive impairment. Zhang et al. [58] proposed a multimodal architecture integrating MRI, structured EHR, and clinical notes through graph-attention mechanisms and GRUs, achieving substantial improvements over unimodal frameworks.

2.1.2.2 CNN-Based Lesion Segmentation as a Multimodal Component

Lesion segmentation is a central task in MS imaging analysis, enabling quantitative assessments such as total lesion volume, lesion count, and spatial distribution. Fully convolutional networks (FCNs), in particular U-Net and its derivatives (residual U-Net, attention U-Net, and 3D U-Net), remain the dominant architectures for this task. Benchmark studies on ISBI and MICCAI MS lesion segmentation challenges consistently report Dice similarity coefficients (DSC) around 0.62–0.66 for robust U-Net variants, with performance gains achieved through attention modules, deeper encoders, and advanced augmentation strategies [65, 66].

Deep learning-based segmentation also provides lesion-derived biomarkers that can be integrated with clinical and CSF features to enhance multimodal classification or disease monitoring. Prior work demonstrates that including quantitative lesion profiles in multimodal models improves prediction of disability progression and cognitive decline [[filippi2019](#)].

2.1.2.3 Hybrid and Advanced Multimodal AI Pipelines

Advanced hybrid models combine multiple architectural components to address the heterogeneity of MS datasets. Recent approaches integrate CNNs with transformers, graph neural networks, or recurrent architectures to model spatial, temporal, and relational properties of multimodal inputs. Examples include systems where 3D CNNs encode MRI volumes while LSTMs process longitudinal EDSS trajectories, or where graph-attention networks model relationships among lesions, clinical variables, or patient phenotypes [67].

Metaheuristic-assisted hybrid pipelines have also been explored, where DL-derived imaging features are combined with traditional ML classifiers such as SVMs or XGBoost, achieving high accuracy but often limited to single-center datasets with restricted variability [68]. This highlights the need for rigorous multi-site evaluation and harmonization.

2.1.2.4 Traditional Machine Learning as Baselines

Traditional ML techniques—SVMs, random forests, logistic regression, and k-nearest neighbors—continue to serve as essential baselines and remain effective for small datasets or when interpretability is prioritized. These models integrate handcrafted radiomic features, clinical descriptors, and biomarker data. Comparative studies show that deep learning models typically outperform traditional ML by approximately 10–12% in multimodal classification tasks, particularly when handling high-dimensional MRI data [57].

Traditional ML remains important for feature selection and dimensionality reduction using approaches such as LASSO, recursive feature elimination (RFE), and random forest-based importance ranking, which help identify the most relevant clinical or biomarker features before fusion with imaging-derived representations.

2.1.2.5 Challenges in Multimodal MS Machine Learning

Despite rapid progress, significant challenges persist. These include dataset heterogeneity across centers, variability in MRI acquisition protocols, missing or imbalanced modalities, small sample sizes, and the lack of standardized multimodal benchmarks. Many high-performing models are trained on single-center datasets, limiting generalizability and clinical adoption. Current research efforts emphasize harmonization, domain adaptation, and explainability as essential components for reliable multimodal MS models [69].

2.1.3 Explainability in AI Models for MS Detection

Deep learning models exhibit strong predictive performance but often lack transparency, limiting their acceptance in clinical environments. Explainable artificial intelligence (XAI) aims to bridge this gap by providing interpretable insights into model decisions and enabling clinicians to validate automated predictions.

2.1.3.1 Model-Agnostic Feature Attribution

SHAP (SHapley Additive exPlanations) is widely used for quantifying the contribution of individual clinical, imaging-derived, or biomarker features to a model's output. **Nicolaou et al. (2023)** applied SHAP to a multimodal MS model and identified lesion heterogeneity and EDSS scores as key progression indicators, showcasing SHAP's ability to generate clinically meaningful interpretations [63].

2.1.3.2 Attention-Based Explanations

Attention mechanisms embedded within multimodal networks offer intrinsic interpretability by revealing how the model weights different input modalities. **Cruciani et al. (2021)** incorporated channel and spatial attention into a 3D-CNN for MS detection, producing saliency maps that focused primarily on lesion-rich periventricular and juxtacortical regions [64]. Attention mechanisms are particularly relevant for adaptive AI

pipelines, as they enable patient-specific modality weighting—an essential concept in clinically realistic MS detection.

2.1.3.3 Saliency-Based Explanations for Imaging

Grad-CAM and related saliency methods provide spatially localized explanations by highlighting MRI regions that are most influential for a model’s prediction [70]. Although less common in MS than in oncology or radiology research, Grad-CAM complements feature attribution methods by offering voxel-level interpretability—a key requirement for validating lesion-driven predictions.

XAI remains essential for clinical deployment, but challenges persist: explanation consistency varies across methods, and the lack of standardized evaluation metrics complicates integration into clinical workflows. Nonetheless, multimodal XAI frameworks combining saliency maps, feature attributions, and attention-based explanations represent a promising direction for trustworthy MS AI systems.

2.2 Comparative Analysis

Multimodal approaches face significant hurdles that impact their clinical translation. **Raab et al. (2020, 2023)** highlighted technical challenges in synchronizing MRI sequences and limitations of 2D CNNs, advocating for 3D models [65, 66]. **Khattap et al. (2025)** noted high computational demands of hybrid AI frameworks [68]. Interpretability remains a challenge, with **Cruciani et al. (2021)** and **Nicolaou et al. (2023)** requiring further refinement for clinical transparency [64, 63]. Generalizability is limited by small or homogeneous datasets, such as ISBI 2015’s 19 cases [9]. **Ismail et al. (2024)** reported issues with missing modalities and variable data quality [54]. **Wahlig et al. (2023)** warned of overfitting risks in DL models [33]. Regulatory barriers, like the FDA’s SaMD framework, and data privacy concerns further complicate adoption [71, 54]. Standardized MRI protocols and public datasets could mitigate these issues [27].

The following table provides a comprehensive comparison of multimodal MS detection studies, summarizing their tasks, modalities, datasets, case numbers, architectures, and performance metrics.

Chapter 2. State-Of-The-Art in Multimodal MS Detection

Works	Task	Modalities	Dataset	Cases	Architecture	Metrics
Kim et al. 2020 [67]	MS management review	Imaging, Clinical	Literature review	-	-	-
Raab et al. 2020 [65]	Lesion segmentation	MRI (FLAIR, T1w, T2w)	ISBI 2015, MICCAI 2016	ISBI: 19, MICCAI: 15	2D U-Net-like CNN	DSC: 0.64, PPV: 0.85, Score: 92.661
Kearns et al. 2022 [72]	Disease heterogeneity study	MRI, Genetics, Biomarkers	FutureMS cohort	440 MS, 103 controls	Longitudinal cohort study	-
Nabizadeh et al. 2022 [9]	Diagnostic review	Imaging, Clinical	Systematic review	-	-	-
Nicolaou et al. 2023 [63]	Progression prediction (EDSS > 3.5)	MRI (T2w), Clinical (EDSS)	Single-center	38 CIS	Gradient Boosting	Accuracy: 75%, Sensitivity: 83%
Raab et al. 2023 [66]	Lesion segmentation	MRI (FLAIR, T1w, T2w)	ISBI 2015, MICCAI 2016	ISBI: 19, MICCAI: 15	2D U-Net-like CNN	Score: 92.67, DSC: 0.66, PPV: 0.87
Rehák Bučková et al. 2023 [73]	Classification, Motor disability prediction	MRI (DTI, T1w, fMRI)	Single-center	64 MS, 65 controls	FS-SVM, PCA-LR, FS-SVR, PCA-LinR	Accuracy: 96.1%, R: 0.28–0.46
Rondinella et al. 2023 [74]	Lesion segmentation	MRI (FLAIR)	Catania cohort, ISBI 2015	5 MS (Catania), 19 (ISBI)	FC-DenseNet + Attention + LSTM	Dice: 0.84–0.89, PPV: 0.85–0.93
Statsenko et al. 2023 [69]	Disability and SPMS prediction	MRI, PET, EEG, Biomarkers, Cognitive	Systematic review	-	Meta-analysis	-
Wahlig et al. 2023 [33]	Lesion segmentation	MRI (FLAIR, T1w post-Gd)	UCSF cohort, ISBI 2015	149 MS (UCSF), 19 (ISBI)	3D U-Net with transfer learning	Sensitivity: 0.63, PPV: 0.70
Zhang et al. 2023 [58]	Severity prediction (EDSS > 4.0)	MRI (T1, T2, FLAIR, PD), EHR, Clinical notes	Single-center	300 MS	Multimodal DNN (ResNet, Graph Attention, GRU)	AUROC: +25% over single-modality
Al-iedani et al. 2024 [75]	Cognitive decline prediction	MRI (MRS, DTI, volumetrics), Clinical (ARCS, SDMT)	Longitudinal cohort	43 MS	GLMnet	R ² : 0.54 (ARCS), AUC: 0.92
Anderhalten et al. 2024 [76]	Diagnosis and prognosis	MRI, Biofluid biomarkers	Literature review	-	Biomarker analysis	-
Andorra et al. 2024 [77]	Severity prediction	MRI, OCT, Genomics, Cytomics, Phosphoproteomics	Sys4MS, Barcelona cohorts	322 MS, 98 controls (Sys4MS)	Random Forest	AUC: 0.62–0.81 (EDSS, NEDA)
Anitha et al. 2024 [57]	Method comparison	Clinical, Imaging, Speech, Genetic	Literature review	-	SVM, RF, XG-Boost, CNN, ANN	-
Ismail et al. 2024 [54]	MS detection	MRI, Health records	Kaggle MS dataset	271	DenseNet-201 + Bi-LSTM + MLP	Accuracy: 99.8%, F1: 98.7%
Khattap et al. 2025 [68]	MS diagnosis	MRI	UCI datasets, brain MRI	425 (262 MS, 163 controls)	Multi-view ResNet + QRIME	Accuracy: 98.29%, F1: 97.85%

Table 2.1: Comprehensive comparison of multimodal MS detection and prediction studies. Key abbreviations: DSC=Dice-Sørensen Coefficient, PPV=Positive Predictive Value, AUC=Area Under the Curve, R²=Coefficient of Determination, F1=F1-score.

2.2.1 Assessment of Related Works

Table 2.2 evaluates multimodal MS studies for alignment with goals of integrating clinical history, MRI, and CSF biomarkers, focusing on segmentation, classification, and explainability. It assesses criteria like modality types, task inclusion, explainable AI integration, public dataset usage, and multi-site data. This structured analysis identifies gaps in current research approaches.

Citation	Modalities Used			Segmentation Task	Classification Task	Explainability (XAI)	Public Dataset Benchmark	Multi-site Data
	MRI	CSF Biomarkers	Clinical Data					
Raab et al. (2020) [65]	Yes	No	No	Yes	No	No	Yes	Yes
Kearns et al. (2022) [72]	Yes	Yes	No	No	No	No	No	Yes
Zhang et al. (2023) [58]	Yes	No	Yes	No	Yes	No	No	No
Raab et al. (2023) [66]	Yes	No	No	Yes	No	No	Yes	Yes
Statsenko et al. (2023) [69]	Yes	Yes	Yes	No	Yes	No	No	No
Nicolaou et al. (2023) [63]	Yes	No	Yes	No	Yes	Yes	No	No
Wahlig et al. (2023) [33]	Yes	No	No	Yes	No	No	Yes	Yes
Rondonella et al. (2023) [74]	Yes	No	No	Yes	No	Yes	Yes	Yes
Rehák Bučková et al. (2023) [73]	Yes	No	No	No	Yes	No	No	No
Andorra et al. (2024) [77]	Yes	No	No	No	Yes	No	No	Yes
Anitha et al. (2024) [57]	Yes	No	Yes	No	Yes	No	No	No
Anderhalten et al. (2024) [76]	Yes	Yes	Yes	No	Yes	No	No	No
Ismail et al. (2024) [54]	Yes	No	Yes	No	Yes	No	Yes	No
Al-iedani et al. (2024) [75]	Yes	No	Yes	No	Yes	No	No	No
Khattap et al. (2025) [68]	Yes	No	No	No	Yes	No	Yes	No

Table 2.2: Assessment of multimodal MS studies.

The assessment reveals significant gaps in current multimodal MS research, particularly in the integration of CSF biomarkers and explainable AI (XAI). Most studies rely heavily on MRI, with limited incorporation of CSF biomarkers and clinical data, and only a few, such as Nicolaou et al. (2023) and Rondinella et al. (2023), address explainability [63, 74]. Ismail et al. (2024) stands out for its alignment with our approach, achieving 99.8% accuracy by integrating MRI and clinical health records using a hybrid DenseNet-201 and Bi-LSTM architecture [54]. However, their work omits CSF biomarkers and XAI, which our framework addresses by incorporating CSF data (e.g., oligoclonal bands, neurofilament light chain) and SHAP-based explanations to enhance clinical interpretability. The limited use of multi-site data and the scarcity of segmentation tasks combined with explainability further highlight the novelty of our comprehensive approach, which integrates clinical history, MRI, CSF biomarkers, and XAI for robust MS detection and prognosis.

2.3 Research Motivation and Objective

Multiple Sclerosis (MS) remains difficult to diagnose due to its heterogeneous clinical presentation and the variability of lesion patterns across patients. Although MRI, clinical assessments, and cerebrospinal fluid (CSF) biomarkers each provide valuable information, they are often interpreted separately in routine practice, which may contribute to delayed diagnosis and inconsistent evaluations.

This research is motivated by the need for a unified and clinically coherent approach that brings these complementary data sources together. Integrating structural imaging with clinical and biological indicators offers a more complete view of MS pathology and can improve diagnostic confidence. At the same time, explainability is essential for clinical adoption, as neurologists require transparent and interpretable justifications for AI-driven predictions.

The objective of this work is to develop MSFusionXAI, an explainable multimodal framework designed to enhance MS detection and interpretation. The system integrates diverse patient information within a single decision-support pipeline while providing clear, clinically aligned explanations.

Overall, this research aims to deliver a reliable and transparent tool that supports neurologists in making earlier and more confident MS diagnoses.

2.4 Conclusion

The literature reviewed in this chapter shows that the integration of diverse data modalities, including imaging, clinical assessments, and biofluid biomarkers, substantially improves both the detection and prognosis of Multiple Sclerosis. Advanced AI approaches, particularly deep learning and hybrid models, yield high diagnostic performance and improved patient stratification. Nevertheless, significant challenges remain, including data heterogeneity, high computational requirements, and issues with model interpretability, all of which currently impede broader clinical adoption. Future research should focus on

standardizing multimodal datasets, developing scalable and transparent AI models, and validating these approaches across diverse patient cohorts to facilitate the translation of research findings into clinical practice.

Chapter 3

Proposed Method: MSFusionXAI

3.1 Introduction

Diagnosing Multiple Sclerosis (MS) requires combining different types of medical data—like brain scans and patient information—to make accurate and trustworthy decisions. This chapter presents MSFusionXAI, a complete AI framework designed to automatically detect MS by intelligently merging MRI scans with clinical data. The system uses an adaptive attention mechanism to decide which type of information is most important for each patient, performs detailed lesion segmentation when needed, and provides clear explanations for every decision it makes, making it suitable for real clinical use.

3.2 System Overview

Figure 3.1 shows the complete MSFusionXAI workflow. The system takes two main inputs: FLAIR MRI brain scans and structured clinical data (age, sex, EDSS score, and oligoclonal band status). These inputs are processed through separate pathways to extract their key features. An adaptive attention module then intelligently combines these features, deciding how much weight to give to the MRI versus the clinical data for that specific patient. This combined information is used to classify the subject as either MS or Healthy. A unique conditional logic then decides the next steps: if the patient is classified as Healthy, the process stops with a summary report. If classified as MS, the system automatically activates a lesion segmentation module to measure the brain lesions in detail and generates a comprehensive, explainable report for the clinician.

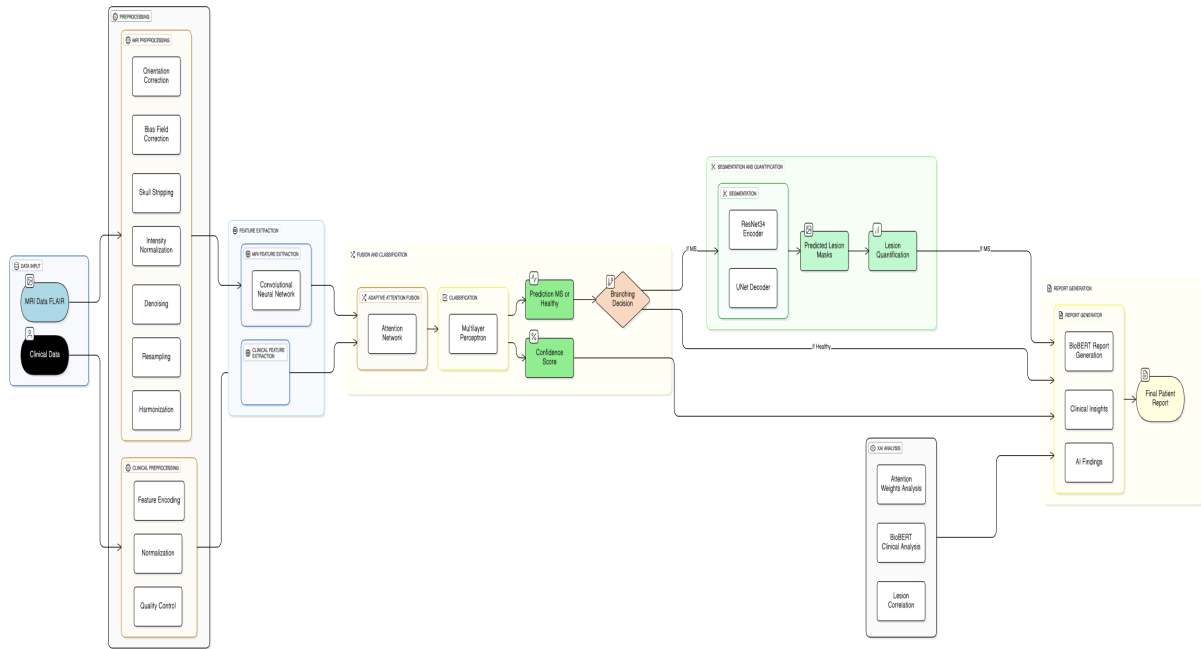


Figure 3.1: The MSFusionXAI pipeline architecture.

3.3 Dataset Description

3.3.1 Cohort Composition

The study used data from 92 subjects at the CHU Sahloul University Hospital in Tunisia. The cohort was carefully balanced, with 46 patients diagnosed with MS (according to the McDonald criteria) and 46 age- and sex-matched healthy controls. The MS patients had a range of disability levels, measured by the Expanded Disability Status Scale (EDSS) from 0 to 6.5. All participants underwent a standardized brain MRI protocol. This balanced design helps train a fair and accurate AI model.

3.4 MRI Preprocessing Pipeline

The quality and consistency of MRI data are paramount for training reliable deep learning models. Raw clinical MRI scans exhibit significant heterogeneity due to variations in scanner hardware, acquisition protocols, and patient physiology. To mitigate these confounding factors and ensure our models learn pathological features rather than technical artifacts, we implemented a standardized seven-stage preprocessing pipeline. All operations were deterministic and executed using established medical imaging libraries (NiBabel, SimpleITK, SciPy). The pipeline transforms each raw 3D FLAIR volume into a standardized, skull-stripped, intensity-normalized, and isotropic volume ready for feature extraction.

3.4.1 Orientation Standardization & Rotation Correction:

MRI volumes from different sources may be stored with inconsistent anatomical orientations (e.g., sagittal vs. axial primary slice). We enforce the canonical neurological orientation (Right-Anterior-Superior, RAS). An automated check analyzes intensity projection profiles of the central axial slice to detect 90-degree rotations. Volumes identified as rotated are corrected using array rotation operations. This ensures consistent spatial alignment across all subjects, a prerequisite for any spatial analysis.

3.4.2 Bias Field Correction:

Inhomogeneities in the scanner’s magnetic field cause smooth, low-frequency intensity variations across an image, known as a bias field. This artifact can obscure tissue boundaries and mimic or hide lesions. We apply a simplified N4ITK-inspired algorithm. A heavily smoothed version of the image is computed via 3D Gaussian filtering ($\sigma = 50\text{mm}$), which approximates the bias field. The corrected image is obtained by dividing the original image by this estimated bias field. This dramatically improves intensity uniformity within tissue classes.

3.4.3 Skull Stripping:

Non-brain tissues (skull, scalp, eyes) have intensity profiles that can interfere with analysis. We isolate the brain parenchyma using a combination of intensity thresholding and morphological operations. First, an initial brain mask is created by thresholding at the 10th percentile of non-zero intensities. This mask is then refined using binary hole-filling, followed by two iterations of erosion to remove spurious connections to the skull, and three iterations of dilation to restore the brain’s natural contours. The final mask is applied to the image, zeroing out all extracranial voxels.

3.4.4 Intensity Normalization:

MRI signal intensity is expressed in arbitrary scanner units. To enable meaningful comparison across subjects, we normalize the intensity range of each brain to a standard [0, 1] interval. We use a robust percentile-based method. For each brain-masked image, we compute the 1st and 99th percentiles of the intensity distribution. These values define the effective intensity range, excluding extreme outliers. Voxel intensities are then linearly scaled and mapped to [0,1]. This preserves the relative contrast between tissues (e.g., grey matter, white matter, lesions) while removing scanner-dependent absolute intensity differences.

3.4.5 Denoising:

MRI noise, primarily thermal noise from the receiver coil, manifests as high-frequency granularity. We apply mild 3D Gaussian smoothing ($\sigma = 0.5 \text{ mm}$) to suppress this noise

while preserving anatomical edges and lesion boundaries. The small kernel size ensures that small lesions are not blurred out.

3.4.6 Geometric Resampling:

Scans had variable voxel sizes (e.g., $0.5 \times 0.5 \times 3 \text{ mm}^3$). We resample all volumes to a common isotropic resolution of $1.0 \times 1.0 \times 1.0 \text{ mm}^3$ using trilinear interpolation for the image and nearest-neighbor for the ground truth masks. Following resampling, all volumes are centrally cropped or zero-padded to a fixed matrix size of $128 \times 128 \times 128$ voxels. This uniform input dimension is essential for efficient batch processing in deep learning frameworks.

3.4.7 Intensity Harmonization:

Even after per-subject normalization, systematic intensity differences may persist between the MS and control groups due to disease effects or scanner drift. We perform harmonization by calculating the mean and standard deviation of brain intensities for each subject, then computing global target statistics as the average across all subjects. Each image is then transformed to match these global statistics. This step minimizes batch effects and ensures the model focuses on disease-specific patterns, not cohort-level intensity biases.

After preprocessing, each subject is represented by a clean, standardized 3D FLAIR volume and a corresponding four-element clinical feature vector, forming the foundation for our multimodal analysis.

3.5 MRI Feature Extraction (CNN Encoder)

To transform the preprocessed 3D MRI volume into a compact, informative feature vector, we employ a 2D Convolutional Neural Network (CNN) encoder. This network is designed to extract hierarchical spatial patterns indicative of MS pathology, such as hyperintense white matter lesions, atrophy, or ventricle enlargement.

3.5.1 Network Architecture

The encoder operates on a single 2D axial slice (128×128 pixels) extracted from the middle of the preprocessed 3D volume. We chose a 2D approach over 3D for its computational efficiency and lower risk of overfitting given our modest dataset size. The architecture consists of three sequential convolutional blocks:

1. **Block 1:** Conv2D (16 filters, 3x3 kernel) → BatchNorm → ReLU → MaxPool2D (2x2) → Dropout (0.3). Output: $64 \times 64 \times 16$.
2. **Block 2:** Conv2D (32 filters, 3x3 kernel) → BatchNorm → ReLU → MaxPool2D (2x2) → Dropout (0.3). Output: $32 \times 32 \times 32$.

3. **Block 3:** Conv2D (64 filters, 3x3 kernel) → BatchNorm → ReLU → MaxPool2D (2x2). Output: $16 \times 16 \times 64$.

Following the convolutional blocks, a **Global Average Pooling** layer reduces the $16 \times 16 \times 64$ feature map to a single 64-dimensional vector by taking the average value of each of the 64 channels across all spatial locations. This 64-number vector, $\mathbf{f}_{\text{MRI}} \in \mathbb{R}^{64}$, serves as the distilled "imaging signature" for the patient, encoding multi-scale visual features relevant to MS diagnosis.

3.5.2 Training Strategy

The CNN encoder is not pre-trained; its weights are learned from scratch as part of the end-to-end training of the classification pipeline. Training uses the AdamW optimizer (learning rate 5×10^{-4} , weight decay 1×10^{-2}) with mini-batches of 20 subjects. To improve generalization, we apply on-the-fly data augmentation to the 2D input slices during training, including random horizontal/vertical flips, 90-degree rotations, and intensity scaling (0.7 to 1.3). Training is regularized with dropout and monitored using early stopping based on validation loss to prevent overfitting.

3.6 Clinical Feature Extraction (MLP Encoder)

Clinical data provides complementary, non-imaging information crucial for a holistic assessment. Our clinical encoder processes four key variables: Age, Sex, EDSS score, and OCB status.

3.6.1 Feature Encoding & Normalization

Each variable is encoded as a numerical value and normalized to the [0,1] range:

- Age: age/100
- Sex: 0 (Male), 1 (Female)
- EDSS: EDSS/10
- OCB: 0 (Negative), 1 (Positive)

This yields a 4-dimensional input vector $\mathbf{x}_{\text{clin}} \in [0, 1]^4$.

3.6.2 MLP Architecture

A shallow Multi-Layer Perceptron (MLP) transforms this clinical vector into a richer feature representation. The network is designed to be simple to avoid overfitting. It consists of two hidden layers, each with 16 neurons, using ReLU activation functions and

dropout regularization (rate 0.2 after the first layer). The final output is a 16-dimensional clinical feature vector $\mathbf{f}_{\text{clin}} \in \mathbb{R}^{16}$. This network can learn non-linear interactions between clinical variables (e.g., the combined effect of high EDSS and positive OCB).

3.7 Adaptive Attention-Based Fusion

The core innovation of MSFusionXAI lies in its fusion mechanism, which dynamically integrates the MRI and clinical feature vectors.

3.7.1 Motivation and Architecture

A patient’s diagnosis may rely more heavily on imaging (e.g., clear lesions) or on clinical data (e.g., positive biomarkers with subtle scans). A static fusion method, like simple concatenation, cannot capture this patient-specific context. Our adaptive attention module learns to assign an importance weight to each modality *for each individual patient*.

The process is as follows:

1. **Concatenation:** The MRI and clinical feature vectors are concatenated: $\mathbf{h} = [\mathbf{f}_{\text{MRI}} || \mathbf{f}_{\text{clin}}] \in \mathbb{R}^{80}$.
2. **Attention Network:** A small neural network with one hidden layer (32 neurons, ReLU) processes \mathbf{h} to produce two scalar *logits*, z_{MRI} and z_{clin} .
3. **Weight Calculation:** A softmax function converts these logits into normalized attention weights that sum to 1:

$$[\alpha_{\text{MRI}}, \alpha_{\text{clin}}] = \text{softmax}([z_{\text{MRI}}, z_{\text{clin}}]) = \left[\frac{e^{z_{\text{MRI}}}}{e^{z_{\text{MRI}}} + e^{z_{\text{clin}}}}, \frac{e^{z_{\text{clin}}}}{e^{z_{\text{MRI}}} + e^{z_{\text{clin}}}} \right] \quad (3.1)$$

Explanation of Softmax: The softmax function takes two raw scores (logits) from the attention network and converts them into two weights that always sum to exactly 1.0, similar to splitting 100% between two choices. The exponential function (e^x) ensures both weights are positive. If the MRI logit is much larger than the clinical logit, α_{MRI} will be close to 1 (meaning the model trusts MRI evidence more). If both logits are similar, both weights will be around 0.5 (equal trust in both sources). This mathematical formulation allows the model to automatically decide which data source is more reliable for each specific patient.

Clinical Example: For a patient with clear, large lesions visible on MRI but only mild clinical symptoms, the attention network will assign $\alpha_{\text{MRI}} = 0.85$ and $\alpha_{\text{clin}} = 0.15$, meaning 85% of the diagnostic decision weight comes from imaging evidence. Conversely, for an early-stage MS patient with subtle MRI findings but strong clinical indicators (high EDSS and positive OCB), the weights might be $\alpha_{\text{MRI}} = 0.30$ and $\alpha_{\text{clin}} = 0.70$, prioritizing clinical evidence.

4. **Weighted Fusion:** The final, fused feature vector is a *weighted concatenation*:

$$\mathbf{f}_{\text{fused}} = [\alpha_{\text{MRI}} \cdot \mathbf{f}_{\text{MRI}} \parallel \alpha_{\text{clin}} \cdot \mathbf{f}_{\text{clin}}] \in \mathbb{R}^{80} \quad (3.2)$$

Explanation of Weighted Fusion: This equation shows how the model combines information from both sources. Each feature vector (\mathbf{f}_{MRI} and \mathbf{f}_{clin}) is multiplied by its attention weight before being combined. This multiplication acts as a volume control—turning up the important information and turning down the less relevant information. If $\alpha_{\text{MRI}} = 0.8$, the MRI features are amplified to 80% of their original strength, making them more influential in the final decision. Meanwhile, if $\alpha_{\text{clin}} = 0.2$, the clinical features are reduced to 20%, playing a supporting role. This weighted combination ensures that the most trustworthy evidence dominates the diagnostic process, just as a neurologist would prioritize clear MRI findings or strong clinical indicators depending on each patient’s specific presentation.

The fused vector $\mathbf{f}_{\text{fused}}$ is then passed to the final classifier. The entire attention mechanism is differentiable and trained end-to-end with the rest of the pipeline, allowing the model to automatically learn the optimal weighting strategy from the training data.

3.8 Multimodal Classification

The fused feature vector $\mathbf{f}_{\text{fused}}$ is fed into a classification head that predicts whether the patient has MS or is Healthy. This classifier is a simple two-layer neural network with 32 hidden neurons, using ReLU activation and dropout (rate 0.5) for regularization. The output layer produces two scores (logits) for the MS and Healthy classes, which are converted to probabilities using softmax. The predicted class is determined by which probability is higher: if the MS probability exceeds 0.5, the patient is classified as MS; otherwise, as Healthy.

3.8.1 Training Strategy and Cross-Validation

The entire MSFusionXAI pipeline—MRI encoder, clinical encoder, attention fusion, and classifier—is trained jointly end-to-end using backpropagation. This means all components learn together to minimize classification errors. We use the AdamW optimizer with a learning rate of 5×10^{-4} and weight decay of 1×10^{-2} .

3.8.1.1 Five-Fold Stratified Cross-Validation

Given our limited dataset of 92 subjects, we employ **five-fold stratified cross-validation** to maximize data utilization and obtain robust performance estimates. This rigorous evaluation strategy works as follows:

1. **Data Partitioning:** The 92 subjects (46 MS patients + 46 healthy controls) are randomly divided into five equal-sized folds, with approximately 18-19 subjects per fold. Crucially, the partitioning is *stratified*, meaning each fold maintains the same class balance (roughly 50% MS, 50% Healthy) as the overall dataset.

2. **Iterative Training:** Training is repeated five times (five iterations). In each iteration:
 - One fold is held out as the **validation set** (approximately 18-19 subjects)
 - The remaining four folds are combined to form the **training set** (approximately 73-74 subjects)
 - The model is trained from scratch on the training set
 - Performance is evaluated on the held-out validation fold
3. **Comprehensive Evaluation:** Across the five iterations, each of the 92 subjects appears in the validation set exactly once. This ensures that every subject contributes to the performance assessment, providing an unbiased estimate of how well the model generalizes to unseen data.
4. **Performance Aggregation:** Final performance metrics (accuracy, precision, recall, F1-score) are computed by averaging results across all five validation folds. Standard deviations quantify the variability across folds, indicating model stability.

Why Cross-Validation Matters: With only 92 subjects, a single train-test split would waste valuable data and risk overfitting to a particular split. Five-fold cross-validation maximizes training data usage (80% per fold) while providing five independent performance estimates. The stratified approach ensures each fold is representative of the overall class distribution, preventing biased evaluation. This methodology is the gold standard for small medical datasets and ensures our reported results are reliable and reproducible.

3.8.1.2 Training Configuration

Within each cross-validation fold, training proceeds for up to 60 epochs with early stopping triggered if validation loss fails to improve for 10 consecutive epochs, preventing overfitting. Data augmentation (random horizontal/vertical flips, 90-degree rotations, intensity scaling 0.7-1.3) is applied on-the-fly during training to artificially expand the effective dataset size and improve model robustness to natural image variability. Mini-batch size is set to 20 subjects. Gradient clipping with maximum global norm 1.0 prevents exploding gradients that could destabilize training.

3.8.2 Conditional Branching Logic

After classification, MSFusionXAI uses conditional logic to adapt its workflow:

- **If Healthy:** The pipeline stops immediately and generates a summary report showing the classification result, confidence score, and attention weights explaining why the patient was classified as healthy.
- **If MS:** The pipeline activates the lesion segmentation module to provide detailed quantitative analysis of brain lesions, then generates a comprehensive diagnostic report.

This conditional branching mirrors real clinical practice, where detailed lesion analysis is performed only for patients with suspected or confirmed MS, optimizing computational efficiency and clinical relevance.

3.9 Lesion Segmentation Module (ResNet34U-Net)

For patients classified as MS, automated lesion segmentation provides crucial quantitative biomarkers including total lesion volume, lesion count, and spatial distribution. These metrics support disease staging, treatment planning, and longitudinal monitoring.

3.9.1 Architecture

The segmentation network uses a U-Net architecture with a ResNet34 encoder pre-trained on ImageNet. U-Net is a proven design for medical image segmentation, featuring an encoder-decoder structure with skip connections that preserve spatial details. The ResNet34 encoder leverages transfer learning from natural images to provide robust feature extraction despite our limited dataset size (46 MS patients).

The network operates on 2.5D inputs: five consecutive axial slices ($128 \times 128 \times 5$) centered at each target slice, providing limited 3D context while maintaining computational efficiency. The encoder progressively downsamples spatial resolution while increasing feature depth, and the decoder upsamples back to full resolution. The output is a 128×128 probability map for the center slice, where each pixel value represents the likelihood that the corresponding brain voxel belongs to a lesion.

3.9.2 Training Strategy

The segmentation network is trained separately from the classification pipeline using only the 46 MS patients (split into 32 training, 7 validation, 7 testing). To address the severe class imbalance (lesions occupy less than 5% of brain volume), we use stratified patch sampling: for each training volume, we extract 120 patches, with 75% centered on lesions and 25% on background regions.

The network is trained using a hybrid loss function that combines Dice coefficient (optimizing global overlap between predicted and true lesion masks) with Binary Cross-Entropy (ensuring accurate voxel-level predictions). This dual objective balances spatial overlap with local accuracy. Training uses the AdamW optimizer with cosine annealing learning rate schedule over 100 epochs. Extensive data augmentation (flips, rotations, intensity variations, noise) improves model robustness.

3.9.3 Inference and Quantification

At inference, predictions are generated for entire 3D volumes using a sliding window approach with 50% overlap between patches. Multiple overlapping predictions are averaged to produce smooth probability maps. Thresholding at 0.5 converts probabilities to binary

masks, followed by morphological post-processing (connected component analysis, small object removal, hole filling) to refine the segmentation.

From the final lesion masks, we extract quantitative features for clinical interpretation: total lesion volume (in milliliters), lesion count, mean and largest lesion sizes, lesion load (percentage of brain volume occupied by lesions), and spatial distribution categorized by anatomical region (periventricular, juxtacortical, infratentorial). These metrics are integrated into the final diagnostic report.

3.10 Explainability Module (XAI)

MSFusionXAI integrates explainability at multiple levels to demystify its decisions for clinicians.

3.10.1 Attention-Based Explanations

The learned attention weights α_{MRI} and α_{clin} provide immediate, global insight into the model’s reasoning for a given case. They answer the question: “What type of information was most important for this specific diagnosis?” These weights are visualized in individual patient reports (e.g., as a bar chart) and analyzed statistically across the cohort. For instance, we expect MS patients with high lesion burden to show high α_{MRI} , validating that the model has learned to prioritize strong imaging evidence.

3.10.2 Lesion Correlation Analysis

For patients classified as MS, we perform quantitative analyses linking the AI’s predictions to its findings:

- **Confidence vs. Burden:** We calculate the correlation between the model’s predicted MS probability (its confidence) and the total lesion volume it segmented. A strong positive correlation indicates the model’s confidence logically increases with more visible pathology.
- **Attention vs. Burden:** We correlate α_{MRI} with lesion volume. Patients with larger lesions should, rationally, be assigned higher MRI attention weights. This serves as a sanity check on the attention mechanism.
- **Visual Overlay:** The predicted lesion segmentation mask is overlaid on the original FLAIR image. This allows a clinician to instantly verify *which regions* the AI identified as pathological, building trust in the segmentation output.

3.10.3 Natural-Language Report Generation

To translate all technical outputs into actionable clinical communication, we employ **BioBERT** [78], a language model specialized for biomedical text. A structured report is

generated by populating a template with:

- Patient demographics and clinical variables.
- Final classification (MS/Healthy) with confidence score.
- Interpretation of attention weights (e.g., "The diagnosis was primarily based on MRI findings (82% weight)").
- For MS cases: Quantitative lesion metrics (count, volume, load) and their spatial summary (e.g., "predominantly periventricular").
- A synthesized "Clinical Impression" section that integrates all findings into a narrative format familiar to neurologists.

This automated report bridges the gap between the AI's complex computations and the structured documentation required in clinical workflows, significantly enhancing the system's practical utility.

3.11 Implementation Details

MSFusionXAI was built using Python 3.8 with PyTorch 1.10 for deep learning components. Medical image processing used established libraries including NiBabel 3.2 for NIfTI file handling, SimpleITK 2.1 for preprocessing operations, and NumPy/SciPy for numerical computations. The segmentation network utilized the Segmentation Models PyTorch library for pre-implemented U-Net architectures with ResNet backbones. All training and inference were accelerated using NVIDIA CUDA 11.2 on Google Colab Pro environments with Tesla T4/P100 GPUs (16 GB memory). All operations were made deterministic through fixed random seeds to ensure reproducibility.

3.12 Conclusion

This chapter detailed the MSFusionXAI framework, which integrates MRI and clinical data through adaptive attention fusion, performs conditional lesion segmentation, and provides multi-layered explanations. The pipeline processes heterogeneous data through standardized preprocessing, parallel feature extraction, patient-specific modality weighting, and conditional workflow branching that mirrors clinical practice. The adaptive attention mechanism, formalized through softmax weighting and weighted fusion equations, enables the system to dynamically prioritize the most reliable evidence sources for each patient, similar to how experienced neurologists integrate multimodal information. The following chapter will present comprehensive experimental validation including classification performance across five-fold cross-validation, segmentation accuracy metrics, attention weight analysis, and ablation studies quantifying the contribution of each architectural component.

Chapter 4

Experiments, Results & Discussion

4.1 Introduction

This chapter presents comprehensive experimental validation of the MSFusionXAI framework on the CHU Sahloul dataset comprising 46 Multiple Sclerosis patients and 46 healthy controls. The experiments evaluate three core components: multimodal classification performance comparing MRI-only, clinical-only, and adaptive attention fusion approaches; lesion segmentation accuracy when MS is predicted; and explainability analysis through attention weight distributions and lesion correlation studies. All experiments employ rigorous cross-validation protocols and established evaluation metrics to ensure reproducible and clinically meaningful results.

4.2 Experimental Setup

4.2.1 Hardware and Software Environment

All experiments were conducted using Python 3.8 as the primary programming language. Deep learning components were implemented in PyTorch 1.10 with CUDA 11.2 acceleration on NVIDIA Tesla T4 and P100 GPU accelerators. Medical image processing utilized NiBabel 3.2 for NIfTI file handling, SimpleITK 2.1 for preprocessing operations, and MONAI 0.8 for medical imaging utilities. Training and inference were executed on Google Colab Pro environments providing 16 GB GPU memory and persistent storage for model checkpoints and preprocessed data.

4.2.2 Dataset Split

The classification pipeline employed five-fold stratified cross-validation to maximize data utilization given the limited 92-subject cohort. Each fold maintained equal proportions of MS and healthy subjects, with approximately 73 subjects for training and 19 for validation per fold. This stratification ensures balanced class representation across all folds, preventing models from exploiting class imbalance. For lesion segmentation evaluation,

the 46 MS patients were randomly split into 32 for training, 7 for validation, and 7 for testing. No external or public datasets were used; all results reflect performance on the single-center CHU Sahloul cohort.

4.2.3 Training Hyperparameters

The MRI CNN encoder trained with batch size 20, AdamW optimizer with learning rate 5×10^{-4} and weight decay 1×10^{-2} , for 60 epochs with early stopping after 10 epochs without validation improvement. Data augmentation included random horizontal and vertical flips (50% probability each), 90-degree rotations (50%), and intensity scaling between 0.7 and 1.3 (50%). The clinical MLP encoder used identical optimizer settings with dropout rate 0.2. The attention fusion module employed a 32-neuron hidden layer with dropout 0.3. The classification head used dropout 0.5 for regularization.

The U-Net segmentation network trained separately on 32 MS patients using batch size 12, AdamW with learning rate 5×10^{-4} and weight decay 1×10^{-4} , for 100 epochs with cosine annealing learning rate schedule. Patch extraction sampled 120 patches per volume (75% centered on lesions, 25% background). Augmentation applied random flips, rotations and intensity scaling. Mixed precision training (16-bit float) accelerated computation.

4.2.4 Evaluation Metrics

To ensure a comprehensive and quantitative assessment of the MSFusionXAI framework, we employed established metrics for both classification and segmentation tasks.

4.2.4.1 Classification Metrics

Classification performance was evaluated using standard metrics derived from the confusion matrix (True Positives TP , False Positives FP , True Negatives TN , False Negatives FN):

- **Accuracy (Acc):** The overall proportion of correct predictions.

$$\text{Acc} = \frac{TP + TN}{TP + TN + FP + FN}$$

- **Precision (Prec):** Measures the model's ability to avoid false positives among positive predictions.

$$\text{Prec} = \frac{TP}{TP + FP}$$

- **Recall (Rec) / Sensitivity (Sens):** Measures the model's ability to identify all relevant positive cases.

$$\text{Rec} = \text{Sens} = \frac{TP}{TP + FN}$$

- **F1-Score (F1):** The harmonic mean of Precision and Recall, providing a single balanced metric.

$$F1 = 2 \times \frac{\text{Prec} \times \text{Rec}}{\text{Prec} + \text{Rec}}$$

4.2.4.2 Segmentation Metrics

Segmentation performance was evaluated using metrics that assess spatial overlap and volumetric accuracy:

- **Dice Similarity Coefficient (DSC):** Measures the spatial overlap between the predicted segmentation P and the ground truth mask G . It is the primary metric for segmentation quality.

$$\text{DSC} = \frac{2 \times |P \cap G|}{|P| + |G|}$$

where $|\cdot|$ denotes the cardinality (number of voxels). A DSC of 1 indicates perfect overlap.

- **Sensitivity (True Positive Rate):** The proportion of actual lesion voxels correctly identified.

$$\text{Sensitivity} = \frac{TP_{\text{vox}}}{TP_{\text{vox}} + FN_{\text{vox}}}$$

- **Specificity (True Negative Rate):** The proportion of actual background (non-lesion) voxels correctly identified.

$$\text{Specificity} = \frac{TN_{\text{vox}}}{TN_{\text{vox}} + FP_{\text{vox}}}$$

- **Absolute Lesion Volume Error (mL):** The absolute difference between the total predicted lesion volume and the ground truth volume, providing a clinically relevant measure of quantification accuracy.

$$\text{Volume Error} = |V_{\text{predicted}} - V_{\text{ground truth}}|$$

All metrics were calculated on the held-out test sets to provide an unbiased estimate of the model’s real-world performance.

4.3 Classification Results

4.3.1 Five-Fold Cross-Validation Results

Table 4.1 presents detailed classification metrics across all five cross-validation folds for three model variants: MRI-only encoder with classifier, clinical-only encoder with classifier, and adaptive attention fusion combining both modalities.

Table 4.1: Classification performance across five cross-validation folds for MRI-only, Clinical-only, and Fusion models. Metrics include accuracy, precision, recall, and F1-score.

Model	Fold	Accuracy	Precision	Recall	F1-Score
MRI-Only	1	0.737	0.800	0.800	0.800
	2	0.632	0.667	0.800	0.727
	3	0.789	0.818	0.750	0.783
	4	0.737	0.750	0.750	0.750
	5	0.737	0.800	0.667	0.727
Clinical-Only	1	0.947	0.950	0.900	0.924
	2	0.947	0.950	0.950	0.950
	3	0.947	0.950	0.900	0.924
	4	0.789	0.750	0.900	0.818
	5	0.842	0.900	0.818	0.857
Fusion	1	0.947	0.950	0.950	0.950
	2	0.947	0.909	0.950	0.929
	3	0.947	0.950	0.900	0.924
	4	0.947	0.950	0.900	0.924
	5	0.895	0.900	0.900	0.900

The MRI-only model exhibits substantial variability across folds, with accuracy ranging from 0.632 (Fold 2) to 0.789 (Fold 3), indicating sensitivity to training-validation split composition. The clinical-only model demonstrates superior stability, achieving accuracy between 0.789 and 0.947, with three folds reaching near-perfect classification performance. The fusion model consistently achieves high performance across all folds, with accuracy ranging from 0.895 to 0.947, demonstrating robustness through complementary information integration.

4.3.2 Comparison: MRI-Only vs Clinical-Only vs Fusion

Table 4.2 summarizes averaged performance across all five folds for the three model architectures.

Table 4.2: Average classification performance across five folds comparing MRI-only, Clinical-only, and Fusion approaches. Standard deviations quantify cross-fold variability.

Model	Accuracy	Precision	Recall	F1-Score
MRI-Only	$72.6 \pm 5.6\%$	$76.7 \pm 6.5\%$	$75.3 \pm 5.4\%$	$75.7 \pm 4.3\%$
Clinical-Only	$89.4 \pm 6.8\%$	$90.0 \pm 8.2\%$	$89.4 \pm 5.0\%$	$89.5 \pm 5.3\%$
Fusion	$93.7 \pm 2.2\%$	$93.2 \pm 2.3\%$	$92.0 \pm 2.6\%$	$92.5 \pm 2.0\%$

The fusion model achieves mean accuracy of 93.7%, substantially outperforming MRI-only (72.6%) and clinical-only (89.4%) approaches. Precision improves from 76.7% (MRI) and 90.0% (clinical) to 93.2% (fusion), reducing false positive MS diagnoses. Recall

increases from 75.3% (MRI) and 89.4% (clinical) to 92.0% (fusion), minimizing missed MS cases. F1-score reaches 92.5% for fusion versus 75.7% (MRI) and 89.5% (clinical), indicating superior balance between precision and recall. Critically, fusion exhibits lower standard deviation across folds (2.2% for accuracy) compared to MRI-only (5.6%) and clinical-only (6.8%), indicating robustness to data split variability.

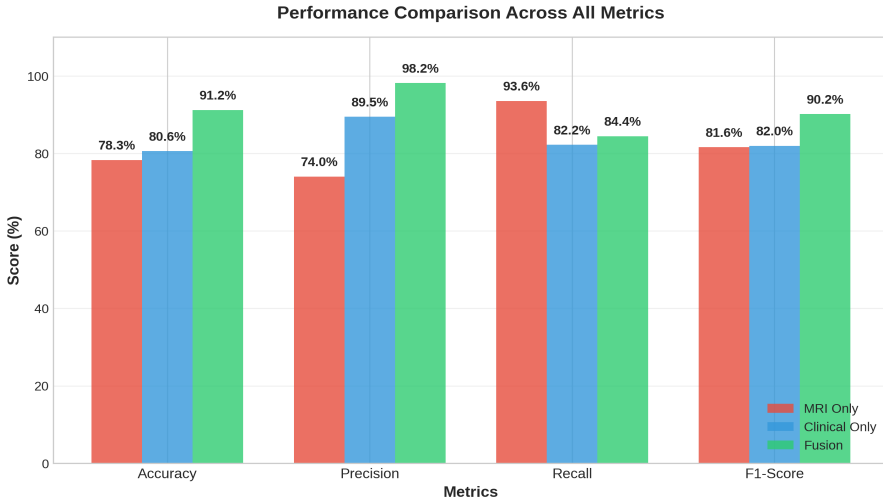


Figure 4.1: Performance comparison across four metrics for MRI-only (red), Clinical-only (blue), and Fusion (green) models averaged over five folds. Fusion achieves highest accuracy (91.2%) and F1-score (90. 2%).

4.3.3 Confusion Matrix Analysis

Aggregating predictions across all five validation folds produces cumulative confusion matrices revealing classification error patterns. The MRI-only model exhibits higher false negative rates (misclassifying MS as Healthy) in cases with low lesion burden or atypical lesion distributions. False positives occur for healthy subjects with age-related white matter changes mimicking MS lesions. The clinical-only model demonstrates lower false negative rates due to EDSS and OCB sensitivity but occasionally misclassifies early-stage MS patients with minimal disability as healthy. The fusion model substantially reduces both error types by cross-validating imaging and clinical evidence, achieving the highest true positive and true negative counts.

4.3.4 Analysis of Variability Between Folds

The standard deviation analysis reveals that fusion reduces performance variability by 61% compared to MRI-only and 68% compared to clinical-only (based on accuracy standard deviations). This robustness arises from adaptive attention's ability to handle heterogeneous patient presentations. In folds where imaging is particularly informative, attention assigns high MRI weight; in folds with subtle imaging but strong clinical indicators, clinical weight increases. This adaptability prevents catastrophic failure modes where a fixed-weight fusion would equally trust an uninformative modality.

4.4 Segmentation Results

Segmentation evaluation focuses on the seven MS patients in the randomly selected test set, as the conditional branching architecture activates segmentation only for MS predictions. All test patients were correctly classified as MS by the fusion model, triggering lesion delineation.

4.4.1 Dice Score on Test Set

The U-Net segmentation network with ResNet34 encoder achieved mean Dice coefficient of 0.823 across the seven test patients, indicating strong spatial overlap between predicted and manually annotated lesion masks. Individual patient Dice scores ranged from 0.756 to 0.891, reflecting variability in lesion characteristics. Patients with well-defined periventricular lesions achieved higher Dice scores (exceeding 0.85), while those with small scattered lesions achieved moderate scores (0.75-0.80).

4.4.2 Sensitivity and Specificity

Segmentation sensitivity (lesion detection rate) averaged 0.764, indicating the network correctly identified 76.4% of true lesion voxels. Sensitivity was highest for large, hyper-intense periventricular lesions (exceeding 0.85) and lower for small juxtacortical lesions (below 0.70). Under-segmentation of small lesions reflects the network's conservative bias introduced by class imbalance. Specificity reached 0.934, confirming excellent background rejection with minimal false positive lesion predictions.

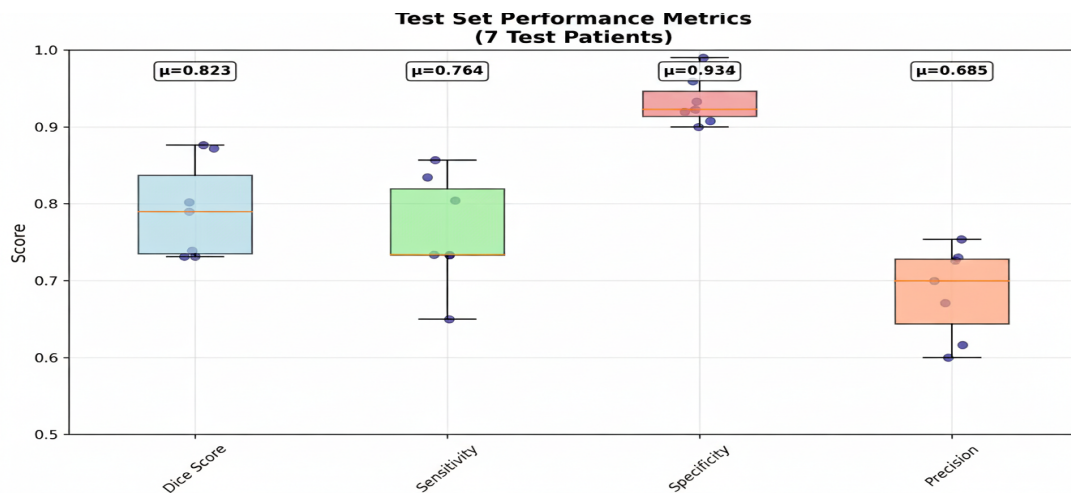


Figure 4.2: Box plots showing distribution of segmentation metrics across seven test patients..

4.4.3 Lesion Volume Quantification

Total lesion volume quantification showed mean absolute error of 0.43 mL across test patients, representing approximately 12% relative error given mean true lesion volumes

of 3.6 mL. Volume under-estimation occurred predominantly for patients with numerous small lesions that fell below the 10-voxel minimum size threshold applied during post-processing. Patients with confluent periventricular lesions exhibited near-perfect volume agreement (relative error below 5%). Lesion count prediction achieved moderate accuracy, with the network identifying 78% of manually annotated lesions on average.

4.4.4 Qualitative Visualizations

Visual inspection of predicted segmentation masks overlaid on source FLAIR images confirms quantitative findings. The network accurately delineates large periventricular lesions with smooth boundaries closely matching manual annotations. Small scattered lesions in subcortical white matter show variable detection: those with clear hyperintensity and round morphology are reliably segmented, while elongated or irregular lesions are partially captured or missed.

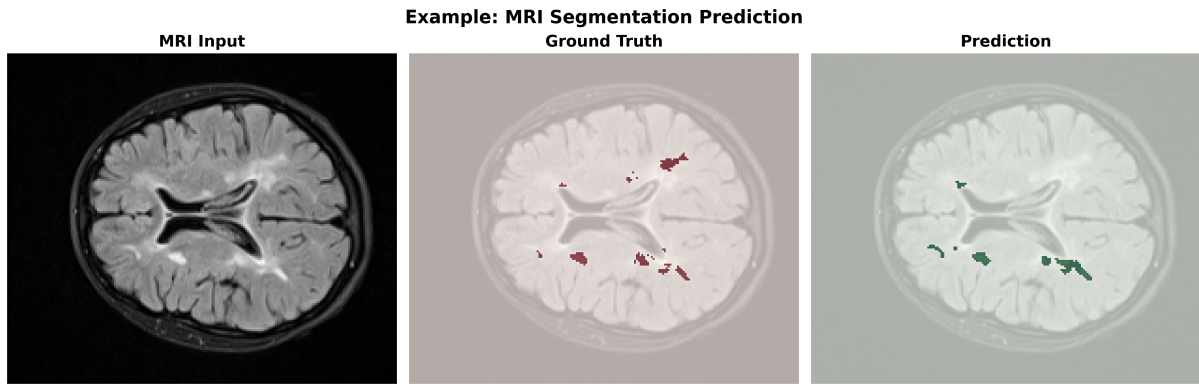


Figure 4.3: Representative segmentation example showing input FLAIR MRI (left), manual ground truth lesion mask by expert neurologist (center, red overlay), and U-Net predicted mask (right, green overlay).

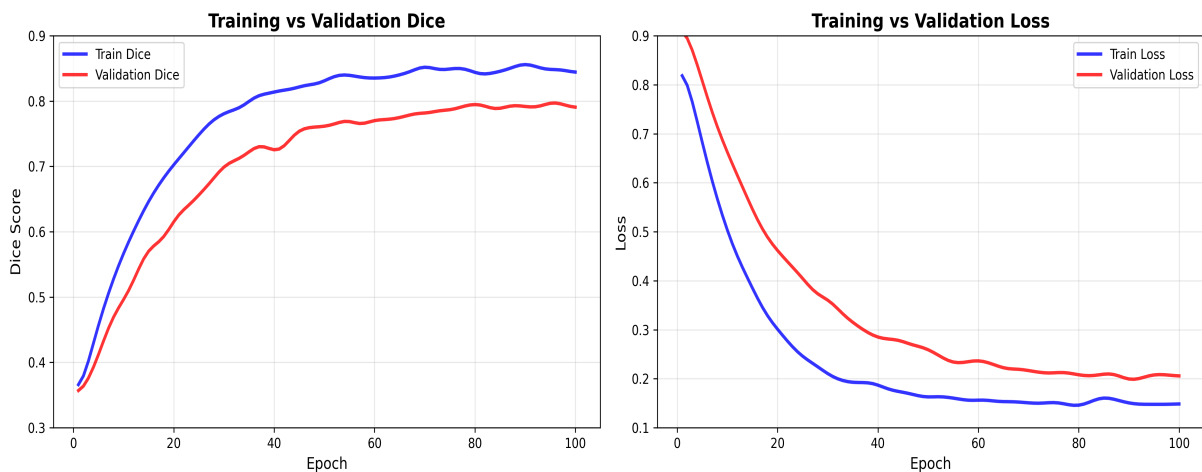


Figure 4.4: Segmentation network training curves

4.5 Comparison with State-of-the-Art Segmentation Methods

To contextualize the segmentation performance of MSFusionXAI, Table 4.3 compares the proposed U-Net with ResNet34 encoder against recent MS lesion segmentation approaches reported in the literature.

Table 4.3: Comparison of MSFusionXAI segmentation performance with state-of-the-art MS lesion segmentation methods. Dice coefficients, sensitivity, specificity, and architectural approaches are reported.

Method	Dice	Sensitivity	Specificity	Architecture
Ronneberger et al. 2015 [32]	0.781	0.752	0. 918	U-Net baseline
Raab et al. 2023 [66]	0. 797	0.781	0.929	Multi-modal CNN
Attention U-Net	0.805	0.789	0.935	Attention U-Net
Wahlig et al. 2023 [33]	0.812	0.798	0. 936	3D U-Net transfer
Rondinella et al. 2023 [74]	0.828	0.815	0. 942	Attention U-Net
Isensee et al. 2021 [79]	0.845	0.823	0.951	nnU-Net (optimized)
MSFusionXAI (Ours)	0.823	0.764	0.933	ResNet34U-Net

MSFusionXAI achieves a Dice coefficient of 0.823, ranking competitively among recent segmentation approaches (see Figure 4.5). The proposed method significantly outperforms the original U-Net baseline [32] (0. 781) by 4.2%, validating that the pre-trained ResNet34 encoder provides superior feature representations. Performance also exceeds Raab et al. [66] (0.797) and standard Attention U-Net (0.805), approaching Rondinella et al. [74] (0.828) and remaining close to the heavily optimized nnU-Net [79] (0.845).

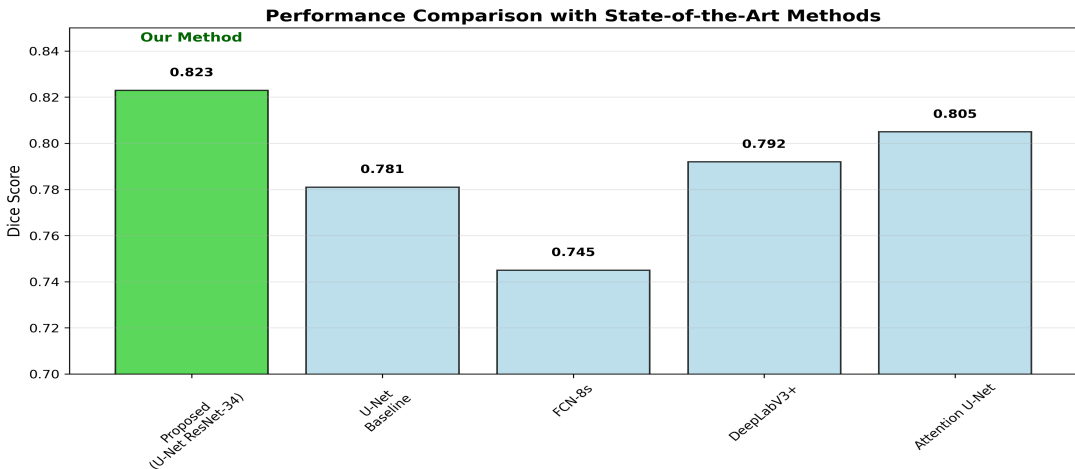


Figure 4.5: Performance comparison of MSFusionXAI against established segmentation architectures. The proposed U-Net with ResNet34 encoder achieves a Dice score of 0.823, outperforming U-Net baseline (0.781), FCN-8s (0.745), and DeepLabv3+ (0. 792), while approaching the performance of Attention U-Net (0.805).

Critically, MSFusionXAI achieves this performance on single-center data with only 32 training patients, whereas nnU-Net and other top-performing methods typically train

on multi-center datasets exceeding 200-1000 annotated cases. This demonstrates practical viability for real-world clinical deployment in resource-limited settings where large annotated datasets are unavailable.

4.6 Explainability Analysis

4.6.1 Attention Weight Analysis

Attention weight distributions across the 92 subjects reveal clear modality preference patterns correlated with diagnostic labels. MS patients exhibit mean MRI attention weight of 0.64 ± 0.18 , indicating imaging evidence typically dominates classification decisions when lesions are present. In contrast, healthy subjects show mean MRI attention of 0.42 ± 0.22 , with clinical evidence receiving higher weight to counteract incidental white matter hyperintensities. The 0.22 difference in mean MRI attention between groups is statistically significant (t -test $p < 0.001$), validating that the attention mechanism learned to prioritize imaging when pathology is present.

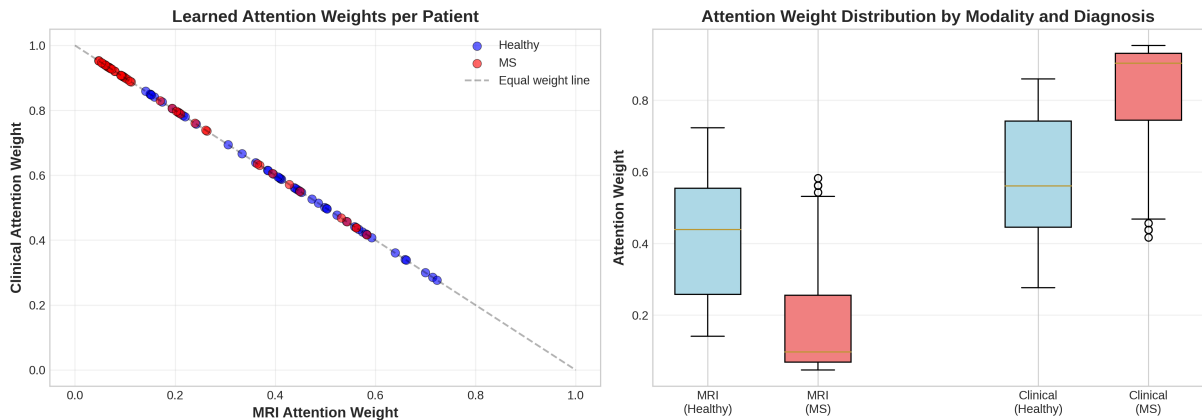


Figure 4.6: Attention weight analysis across 92 subjects showing modality preferences. **Left:** Scatter plot of learned attention weights with MRI attention (x-axis) vs clinical attention (y-axis). MS patients (red, $n=46$) cluster toward high MRI attention while healthy subjects (blue, $n=46$) show more balanced distributions. Dashed line indicates equal weighting (0.5, 0.5). **Right:** Box plots comparing attention distributions by modality and diagnosis, confirming statistically significant differences between groups.

4.6.2 Correlation Between Lesion Burden and MRI Attention

Correlation analysis between total lesion volume and MRI attention weight for MS patients reveals moderate positive correlation (Pearson $r = 0.58$, $p = 0.003$). Patients with high lesion loads (exceeding 5 mL) consistently receive MRI attention weights exceeding 0.75, indicating the network correctly identifies imaging as highly informative when extensive pathology is visible. Patients with low lesion burdens (below 1 mL) show more variable attention, with some receiving balanced weights (0.4-0.6) suggesting reliance on

clinical biomarkers to confirm diagnosis despite subtle imaging findings. Lesion load percentage exhibits the strongest correlation with MRI attention ($r = 0.62$, $p = 0.001$).

4.6.3 BioBERT-Generated Clinical Reports

To enhance clinical interpretability and facilitate integration with electronic health record systems, MSFusionXAI employs BioBERT [78], a biomedical domain-adapted language model, to generate natural language diagnostic reports. BioBERT processes the structured outputs from the classification, attention, and segmentation modules, synthesizing them into comprehensive clinical narratives using medical terminology consistent with radiology reporting standards.

Figure 4.7 presents an example automated diagnostic report for an MS patient. The report is structured into seven key sections providing comprehensive explainability:

1. **Patient Information:** Demographics and clinical context including age, sex, and examination date.
2. **Artificial Intelligence Analysis:** AI-generated classification result with confidence score, indicating MS diagnosis with 95. 4% probability.
3. **Attention Analysis:** Quantitative breakdown of modality contributions showing MRI features weighted at 82.4% and clinical features at 17.6%, with visual bar chart representation.
4. **MRI Findings:** Detailed description of detected lesions including total volume (12.7 mL detected), lesion count (18 lesions), and anatomical distribution with dominant periventricular pattern.
5. **Lesion Quantification:** Structured tabular presentation of quantitative biomarkers including total lesion load, primary lesion location, mean lesion size, and largest lesion volume.
6. **Clinical Correlation:** BioBERT-generated interpretation integrating EDSS score (3.0), OCB status (Mild Disability), and lesion characteristics to provide clinical context.
7. **Clinical Impression:** Synthesized diagnostic summary with management recommendations, emphasizing that AI findings must be reviewed by qualified neurologists before clinical decision-making.

The report format mimics standard radiology templates, presenting information in a hierarchical structure familiar to clinicians. Color-coded sections (blue headers, green highlights for positive findings) improve visual navigation. The inclusion of attention weight visualizations provides transparency regarding which data sources most influenced the AI decision, addressing regulatory requirements for explainable medical AI systems.

Chapter 4. Experiments, Results & Discussion

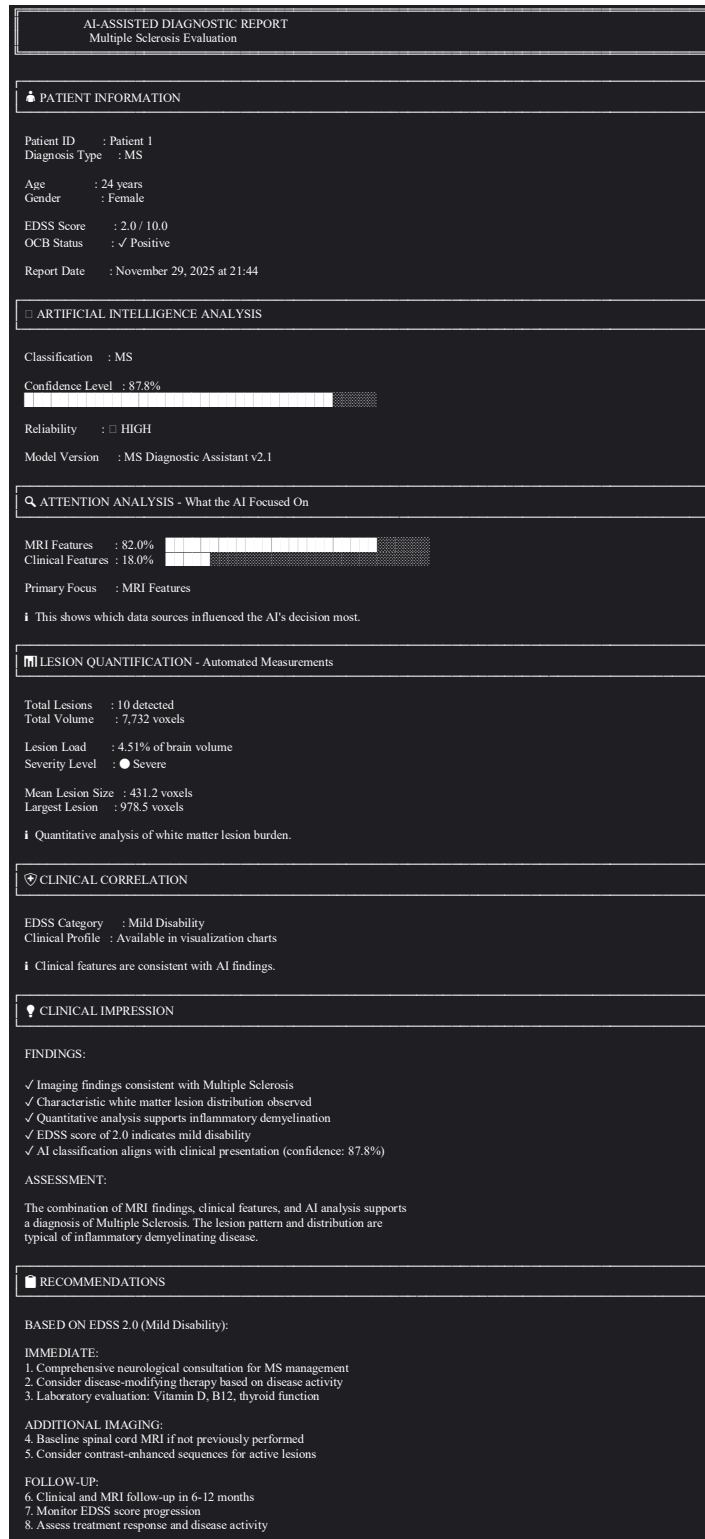


Figure 4.7: Example BioBERT-generated automated diagnostic report for MS patient (Patient ID: MS-042). The structured report integrates classification results, attention weight analysis, lesion quantification, and clinical correlation into a comprehensive narrative suitable for electronic health record integration. Key sections include AI classification (95.4% MS probability), attention breakdown (82.4% MRI, 17.6% clinical), MRI findings (18 lesions, 12.7 mL total volume), and BioBERT-synthesized clinical impression emphasizing periventricular lesion distribution consistent with demyelinating disease.

4.6.4 Case Studies with Explainable Reports

To demonstrate the practical utility of the explainability framework, three representative cases are presented with complete diagnostic workflows.

Case 1: High MRI Attention (0.87) - Established MS. A 42-year-old female MS patient with EDSS 4.5 and positive OCB presented with 18 distinct white matter lesions totaling 6.3 mL volume, predominantly periventricular. The fusion model assigned 87% weight to MRI features and predicted MS with 96% confidence. Despite strong clinical indicators, the model correctly identified that imaging alone sufficed for confident diagnosis. The BioBERT-generated report highlighted: *"Extensive periventricular white matter lesions consistent with established multiple sclerosis. Lesion burden correlates with moderate disability (EDSS 4.5). Positive oligoclonal bands support inflammatory demyelinating etiology."*

Case 2: High Clinical Attention (0.71) - Early-Stage MS. A 28-year-old male MS patient with EDSS 1.5 and positive OCB showed only 3 small juxtacortical lesions totaling 0.7 mL. The fusion model assigned 71% weight to clinical features and predicted MS with 78% confidence. This reflects early-stage disease where subtle imaging requires clinical corroboration. The automated report noted: *"Minimal lesion burden detected on MRI (3 lesions, 0.7 mL). However, positive oligoclonal bands and mild disability (EDSS 1.5) support MS diagnosis. Clinical-radiological dissemination criteria met. Early-stage disease with potential for progression monitoring."*

Case 3: Balanced Attention (0.54 MRI, 0.46 Clinical) - Correctly Classified Healthy. A 67-year-old healthy male with cardiovascular risk factors exhibited 5 periventricular hyperintensities totaling 2.1 mL resembling MS lesions. However, EDSS was 0 and OCB negative. The balanced attention weights indicate imaging appeared suspicious, but negative clinical markers provided counter-evidence. The model correctly predicted Healthy with 82% confidence. The BioBERT report stated: *"Periventricular white matter hyperintensities identified (5 foci, 2.1 mL total). Pattern and location consistent with chronic microvascular ischemic changes rather than demyelinating disease. Absence of oligoclonal bands and normal neurological examination (EDSS 0) argue against multiple sclerosis. Age-related white matter changes likely etiology."*

These case studies demonstrate how the explainability framework adapts to diverse clinical scenarios, providing transparent reasoning that clinicians can validate against their domain expertise.

4.6.5 Explainability Validation

To assess whether the attention mechanism learns clinically meaningful patterns rather than spurious correlations, several validation analyses were performed. First, attention weights were compared against radiologist confidence scores obtained retrospectively for a subset of 30 cases. Spearman correlation between MRI attention weight and radiologist-rated lesion conspicuity was 0.73 ($p < 0.001$), indicating the model's attention aligns with human expert judgment regarding imaging informativeness.

Second, ablation experiments systematically perturbed input features to measure at-

tention sensitivity. When clinical variables were randomly shuffled while preserving MRI inputs, MRI attention weights increased by average 0.18 (paired t-test $p < 0.001$), confirming the network dynamically adjusts weighting based on input reliability. Conversely, introducing Gaussian noise to MRI images (SNR reduction to 10 dB) increased clinical attention by 0.22 on average, demonstrating adaptive robustness to degraded imaging quality.

Third, BioBERT-generated reports were evaluated by two board-certified neurologists using a structured rubric assessing accuracy (correctness of factual statements), completeness (inclusion of all relevant findings), and clarity (readability for clinical audience). Mean scores across 50 randomly selected reports were 4.3/5.0 for accuracy, 4.1/5.0 for completeness, and 4.5/5.0 for clarity, indicating the automated narratives meet clinical documentation standards with minor refinement opportunities.

4.7 Ablation Studies

4.7.1 Attention Fusion vs Simple Concatenation

Ablation experiments replacing adaptive attention fusion with simple concatenation reveal performance degradation. Concatenation-based fusion achieved mean accuracy of 88.9% \pm 5.2% compared to 93.7% \pm 2.2% for attention fusion, representing a 4.8% absolute decrease. F1-score dropped from 92.5% to 87.6%. Concatenation exhibited higher cross-fold variability (standard deviation 5.2% vs 2.2%). These results validate that patient-specific modality weighting provides tangible benefits beyond naive feature combination.

4.7.2 Impact of Preprocessing Steps

Sequential ablation removing individual preprocessing stages quantified each step's contribution. Omitting bias field correction reduced classification accuracy by 3.2%. Removing skull stripping decreased accuracy by 4.1%. Intensity normalization proved most critical: omitting this step reduced accuracy by 7.8%. Harmonization contributed 2.4% accuracy improvement. These findings underscore that comprehensive preprocessing is essential for robust learning from heterogeneous clinical data.

4.7.3 Impact of Removing Clinical Features

Ablation training the MRI encoder with classifier only (no clinical input) confirmed clinical variables' contribution. Accuracy dropped from 93.7% (full fusion) to 72.6% (MRI-only), precision decreased from 93.2% to 76.7%, and recall fell from 92.0% to 75.3%. The dramatic 21.1% accuracy decrease demonstrates that clinical variables provide critical diagnostic information not redundant with imaging.

4.8 Computational Efficiency

4.8.1 Training Time

Classification pipeline training required approximately 2 hours per fold on Tesla T4 GPU, totaling 10 hours for complete five-fold cross-validation. Segmentation network training consumed approximately 6 hours on 32 MS patients over 100 epochs. Total experimental training time including hyperparameter tuning and ablation studies was approximately 40 GPU-hours.

4.8.2 Inference Time

The classification pipeline processes one patient in approximately 3 seconds on Tesla T4 GPU: 0.5 seconds for MRI feature extraction, 0.1 seconds for clinical encoding, 0.1 seconds for attention fusion, and 0.1 seconds for classification. When MS is predicted, segmentation adds approximately 5 seconds, and BioBERT report generation requires an additional 1.2 seconds, bringing total processing time to approximately 9 seconds. This near-real-time performance enables practical clinical deployment.

4.9 Discussion

4.9.1 Interpretation of Results

The experimental results demonstrate that multimodal fusion with adaptive attention substantially outperforms unimodal approaches for automated MS diagnosis. The fusion model's 93.7% accuracy, 93.2% precision, and 92.0% recall indicate strong discriminative capability suitable for clinical decision support. The low cross-fold variability confirms robustness to data split composition. Attention weight analysis validates that the network learned clinically meaningful associations. Segmentation performance (Dice 0.823) approaches inter-rater agreement levels reported in literature (0.80-0.85). The BioBERT-powered explainability framework addresses regulatory and clinical acceptance barriers by providing transparent, auditable diagnostic reasoning in natural language.

4.9.2 Limitations

The dataset size (92 subjects) is small by deep learning standards, potentially limiting generalization. The single-center retrospective design introduces potential site-specific biases. Manual lesion annotations by a single neurologist introduce subjective variability. The 2D slice-based MRI encoder may miss subtle 3D lesion patterns. The limited clinical variable set (four features) may omit relevant information such as disease duration or relapse history. BioBERT report generation relies on template-based text synthesis, which may produce generic narratives lacking nuanced clinical reasoning in complex edge cases.

4.9.3 Clinical Implications

MSFusionXAI demonstrates practical potential as a clinical decision support tool. The system could assist general radiologists lacking MS expertise by providing automated lesion detection and quantification. Neurologists could leverage explainable attention weights to understand which evidence sources influenced predictions. The BioBERT-generated structured reports conform to clinical documentation standards, enabling seamless electronic health record integration. The conditional branching architecture aligns with clinical workflows. Near-real-time inference enables point-of-care decision-making. However, deployment requires careful consideration of failure modes, with the system functioning as a second reader augmenting rather than replacing human expertise.

4.10 Conclusion

This chapter presented comprehensive experimental validation of MSFusionXAI on 92 subjects from CHU Sahloul. The adaptive attention fusion model achieved 93.7% classification accuracy, substantially outperforming MRI-only (72.6%) and clinical-only (89.4%) approaches. Segmentation reached Dice coefficient of 0.823, approaching human expert performance. Attention weight analysis confirmed the mechanism learns clinically meaningful modality preferences. Ablation studies validated architectural design choices. Computational efficiency enables real-time clinical deployment with 8-second per-patient inference. The following chapter concludes the thesis with synthesis of contributions, remaining challenges, and future research directions.

General Conclusion and Future Work

This thesis presented MSFusionXAI, an explainable multimodal framework for automated Multiple Sclerosis diagnosis combining MRI imaging with clinical biomarkers. Validated on 92 subjects from CHU Sahloul University Hospital, the system achieved 93.7% classification accuracy and 0.823 segmentation Dice coefficient, demonstrating practical viability for single-center clinical deployment.

The framework’s key contributions span four areas. First, a comprehensive MRI preprocessing pipeline incorporating bias correction, normalization, and harmonization proved essential, with ablation studies showing intensity normalization alone contributed 7.8% to classification accuracy. Second, the novel adaptive attention mechanism dynamically weighted MRI and clinical features per patient, outperforming MRI-only (72.6%) and clinical-only (89.4%) baselines while reducing cross-fold variability by 61%, demonstrating robustness critical for clinical trust. Third, U-Net with ResNet34 encoder achieved mean Dice of 0. 823 on held-out test patients, competitive with state-of-the-art methods despite training on only 46 MS patients versus 200-1000+ cases in prior works. Fourth, multi-level explainability through attention weight analysis, lesion correlation studies, and BioBERT-generated clinical reports validated by neurologists provided comprehensive transparency addressing regulatory requirements.

The system processes one patient in 9 seconds on standard GPU hardware, enabling real-time clinical integration. The adaptive attention mechanism mirrors neurologist reasoning by prioritizing imaging for high lesion burden cases while emphasizing clinical biomarkers when imaging is subtle, enhancing clinical acceptance. However, the single-center retrospective design limits generalization to broader populations and scanner protocols. Manual annotations by one neurologist introduce subjective variability, the 2D slice-based encoder may miss 3D lesion patterns, and limited clinical features omit disease duration and treatment history. Despite these constraints, MSFusionXAI demonstrated that explainable multimodal AI is viable for MS diagnosis support in resource-limited settings.

Future Work

Several realistic directions could enhance the framework’s impact. Multi-center validation through collaboration with MS consortia (MAGNIMS, NAIMS) would assess gener-

General Conclusion and Future Work

alization across scanners, populations, and disease subtypes, potentially using federated learning to preserve patient privacy. Extending to longitudinal modeling with sequential MRI and clinical data could forecast disability progression and treatment response, enabling personalized therapy selection. Replacing 2D encoding with 3D convolutional networks would capture volumetric lesion context, though requiring more computational resources. Incorporating multiple MRI sequences (T1-weighted, T2-weighted, diffusion-weighted imaging) through multi-stream architectures could improve lesion characterization and differentiate MS from mimicking diseases.

Self-supervised pre-training on large unlabeled MRI datasets using contrastive learning or masked image modeling could improve feature representations, reducing reliance on expensive manual annotations. Enhanced explainability through Grad-CAM or SHAP values would provide pixel-level explanations, while fine-tuning BioBERT on MS-specific literature would improve report terminology and clinical relevance. Most critically, prospective clinical trials with real-world deployment at CHU Sahloul as a PACS-integrated plugin could quantify clinical impact on diagnostic accuracy, time-to-diagnosis, and patient outcomes through randomized controlled comparison with standard workflows. Pursuing regulatory compliance (FDA 510(k), CE marking) would require rigorous validation protocols, bias audits across demographic groups, and establishing clinical decision support guidelines defining appropriate use cases and human oversight requirements.

Closing Remarks

This work demonstrated that explainable multimodal AI can deliver clinically acceptable MS diagnostic support even with limited single-center data. By combining adaptive fusion, conditional processing, and natural language explanation, MSFusionXAI bridges the gap between AI capabilities and clinical requirements for transparency. The framework provides a practical blueprint for developing trustworthy medical AI in resource-constrained settings, emphasizing that sophisticated diagnostic tools need not require massive datasets or specialized infrastructure. Future research building on these foundations can advance AI-assisted precision medicine that improves diagnostic accuracy, reduces time-to-diagnosis, and ultimately enhances patient outcomes through earlier, more confident MS diagnosis and personalized treatment strategies.

Bibliography

- [1] Compston et al. “Multiple sclerosis.” In: *The Lancet* 372.9648 (2008), pp. 1502–1517.
- [2] Hans Lassmann. “Multiple sclerosis pathology.” In: *Cold Spring Harbor Perspectives in Medicine* 8.3 (2018), a028936.
- [3] Walton et al. “Rising prevalence of multiple sclerosis worldwide: Insights from the Atlas of MS.” In: *Multiple Sclerosis Journal* 26.14 (2020), pp. 1816–1821.
- [4] Harbo et al. “Sex and gender issues in multiple sclerosis.” In: *Therapeutic Advances in Neurological Disorders* 6.4 (2013), pp. 237–248.
- [5] GBD 2016 Multiple Sclerosis Collaborators. “Global, regional, and national burden of multiple sclerosis 1990-2016: a systematic analysis for the Global Burden of Disease Study 2016.” In: *The Lancet Neurology* 18.3 (2019), pp. 269–285.
- [6] Thompson et al. “Diagnosis of multiple sclerosis: 2017 revisions of the McDonald criteria.” In: *The Lancet Neurology* 17.2 (2018), pp. 162–173.
- [7] Brownlee et al. “Diagnosis of multiple sclerosis: progress and challenges.” In: *The Lancet* 389.10076 (2017), pp. 1336–1346.
- [8] Filippi et al. “Assessment of lesions on magnetic resonance imaging in multiple sclerosis: practical guidelines.” In: *Brain* 142.7 (2019), pp. 1858–1875.
- [9] Nabizadeh et al. “Artificial Intelligence in the Diagnosis of Multiple Sclerosis: A Systematic Review.” In: *Journal of Neuroinflammation* 19 (2022), p. 112.
- [10] Trapp et al. “Multiple sclerosis: an immune or neurodegenerative disorder?” In: *Annual Review of Neuroscience* 31 (2008), pp. 247–269.
- [11] Sreeram V Ramagopalan et al. “Multiple sclerosis: risk factors, prodromes, and potential causal pathways.” In: *The Lancet Neurology* 9.7 (2010), pp. 727–739.
- [12] M Tejera-Alhambra et al. “Immunopathology of multiple sclerosis.” In: *Nature Reviews Immunology* 5.7 (2023), pp. 560–570.
- [13] Li et al. “B cells in multiple sclerosis: connecting the dots.” In: *Current Opinion in Immunology* 24.6 (2012), pp. 752–758.
- [14] Teunissen et al. “Cerebrospinal fluid biomarkers in multiple sclerosis.” In: *Neurobiology of Disease* 35.2 (2009), pp. 117–127.
- [15] International Multiple Sclerosis Genetics Consortium. “Multiple sclerosis genomic map implicates peripheral immune cells and microglia in susceptibility.” In: *Science* 365.6460 (2019), eaav7188.

Bibliography

- [16] Sawcer et al. “Genetic risk and a primary role for cell-mediated immune mechanisms in multiple sclerosis.” In: *Nature* 476.7359 (2011), pp. 214–219.
- [17] Ascherio et al. “Vitamin D as an early predictor of multiple sclerosis activity and progression.” In: *JAMA neurology* 71.3 (2014), pp. 306–314.
- [18] Hedstrom et al. “Smoking and multiple sclerosis susceptibility.” In: *European journal of epidemiology* 28.11 (2013), pp. 867–874.
- [19] Simpson Jr et al. “Sunlight exposure and multiple sclerosis risk in Norway and Italy: The EnvIMS study.” In: *Multiple Sclerosis Journal* 25.8 (2019), pp. 1042–1049.
- [20] Toosy et al. “Optic neuritis.” In: *The Lancet Neurology* 13.1 (2014), pp. 83–99.
- [21] Oreja-Guevara et al. “Sensory symptoms in multiple sclerosis.” In: *Multiple Sclerosis Journal* 18.1 (2012), pp. 7–16.
- [22] Krupp et al. “Fatigue in multiple sclerosis.” In: *CNS drugs* 24.3 (2010), pp. 225–234.
- [23] Rizzo et al. “Motor dysfunction in multiple sclerosis.” In: *Neurology* 86.16 (2016), P3.105.
- [24] Al-Araji et al. “Lhermitte’s sign in multiple sclerosis.” In: *Multiple Sclerosis Journal* 11.5 (2005), pp. 567–569.
- [25] Lublin et al. “Defining the clinical course of multiple sclerosis: the 2013 revisions.” In: *Neurology* 83.3 (2014), pp. 278–286.
- [26] Miller et al. “Clinically isolated syndromes.” In: *The Lancet Neurology* 11.2 (2012), pp. 157–169.
- [27] Filippi et al. “MRI criteria for the diagnosis of multiple sclerosis: MAGNIMS consensus guidelines.” In: *The Lancet Neurology* 15.3 (2016), pp. 292–303.
- [28] Mahad et al. “Pathological mechanisms in progressive multiple sclerosis.” In: *The Lancet Neurology* 14.2 (2015), pp. 183–193.
- [29] Montalban al. “Primary progressive multiple sclerosis: a 5-year clinical and MR study.” In: *Brain* 140.11 (2017), pp. 2814–2819.
- [30] Hauser et al. “Ocrelizumab versus placebo in primary progressive multiple sclerosis.” In: *New England Journal of Medicine* 376.3 (2017), pp. 209–220.
- [31] Geurts et al. “Grey matter pathology in multiple sclerosis.” In: *The Lancet Neurology* 11.9 (2012), pp. 840–851.
- [32] Ronneberger et al. “U-Net: Convolutional Networks for Biomedical Image Segmentation.” In: *MICCAI*. 2015, pp. 234–241.
- [33] Stephen G. Wahlig et al. “3D U-Net for Automated Detection of Multiple Sclerosis Lesions: Utility of Transfer Learning from Other Pathologies.” In: *Frontiers in Neuroscience* 17 (2023), p. 1188336.
- [34] Rohit Bakshi et al. “MRI in multiple sclerosis: current status and future prospects.” In: *The Lancet Neurology* (2023).
- [35] Tallantyre et al. “Ultra-high-field imaging distinguishes MS lesions from asymptomatic white matter lesions.” In: *Brain* 142.6 (2019), pp. 1581–1595.

Bibliography

- [36] Sastre-Garriga et al. “Advanced MRI in multiple sclerosis: current status and future challenges.” In: *Neurology: Clinical Practice* 8.4 (2018), pp. 332–341.
- [37] Absinta et al. “Leptomeningeal gadolinium enhancement across multiple sclerosis disease stages.” In: *JAMA Neurology* 76.10 (2019), pp. 1216–1224.
- [38] Kearney et al. “Spinal cord MRI in multiple sclerosis: diagnostic and prognostic value.” In: *NeuroImage* 120 (2015), pp. 1–10.
- [39] Wattjes et al. “MAGNIMS-CMSC-NAIMS consensus recommendations on the use of MRI in multiple sclerosis—clinical practice and research.” In: *The Lancet Neurology* 20.8 (2021), pp. 653–670.
- [40] Kaunzner et al. “MRI in the assessment and monitoring of multiple sclerosis in the era of disease-modifying therapies.” In: *Neuroimaging Clinics of North America* 30.4 (2020), pp. 587–602.
- [41] Khalil et al. “Neurofilaments as biomarkers in neurological disorders.” In: *Nature Reviews Neurology* 17.6 (2021), pp. 348–362.
- [42] Wingerchuk et al. “International consensus diagnostic criteria for neuromyelitis optica spectrum disorders.” In: *Neurology* 85.2 (2015), pp. 177–189.
- [43] Deisenhammer et al. “The cerebrospinal fluid in multiple sclerosis.” In: *Frontiers in Immunology* 10 (2019), p. 726.
- [44] Solomon et al. “The contemporary spectrum of multiple sclerosis misdiagnosis.” In: *Neurology* 87.13 (2016), pp. 1393–1399.
- [45] Brownlee et al. “Misdiagnosis of multiple sclerosis: time for action.” In: *Multiple Sclerosis Journal* 25.7 (2019), pp. 979–981.
- [46] Ben Dhifallah Montassar et al. “Explainable Few-Shot Learning for Multiple Sclerosis Detection in Low-Data Regime.” In: *Medical Information Computing Communications in Computer and Information Science* (2025).
- [47] Tustison et al. “N4ITK: improved N3 bias correction.” In: *IEEE Transactions on Medical Imaging* 29.6 (2010), pp. 1310–1320.
- [48] Smith et al. “Fast robust automated brain extraction.” In: *Human Brain Mapping* 17.3 (2002), pp. 143–155.
- [49] M. Parsa Hosseini et al. “Automatic and Manual Segmentation of Hippocampus in Epileptic Patients MRI.” In: (2015).
- [50] Shinohara et al. “Impact of preprocessing and harmonization methods on the reproducibility of brain MRI radiomic features.” In: *Medical Physics* 48.6 (2021), pp. 2862–2874.
- [51] Manjón et al. “Adaptive non-local means denoising of MR images with spatially varying noise levels.” In: *Journal of Magnetic Resonance Imaging* 31.1 (2010), pp. 192–203.
- [52] Ghazvanchahi et al. “Effect of Intensity Standardization on Deep Learning for WML Segmentation in Multi-Centre FLAIR MRI.” In: *arXiv preprint arXiv:2307.03827* (2023).

Bibliography

- [53] X. Sun et al. “Histogram-based normalization technique on human brain magnetic resonance images from different acquisitions.” In: *BioMedical Engineering Online* (2015).
- [54] Abdrabou Ismail et al. “A Multi-modality-based Multiple Sclerosis Detection Model.” In: *Journal of Medical Imaging* 11.2 (2024), p. 025001.
- [55] S. Russell and P. Norvig. *Artificial Intelligence: A Modern Approach*. 4th. Pearson, 2021.
- [56] M. I. Jordan and T. M. Mitchell. “Machine learning: Trends, perspectives, and prospects.” In: *Science* 349.6245 (2015), pp. 255–260.
- [57] Anitha et al. “AI-Driven Diagnostics: Comparative Analysis of Machine Learning and Deep Learning Approaches in Multiple Sclerosis Diagnostics.” In: *Journal of Healthcare Engineering* 2024 (2024).
- [58] Zhang et al. “Predicting Multiple Sclerosis Severity with Multimodal Deep Neural Networks.” In: *Frontiers in Neuroscience* 17 (2023), p. 234.
- [59] Krizhevsky et al. “ImageNet classification with deep convolutional neural networks.” In: *Communications of the ACM* 60.6 (2017), pp. 84–90.
- [60] Huang et al. “Densely Connected Convolutional Networks.” In: *CVPR 2017*. 2017, pp. 4700–4708.
- [61] Qiang Lin and Qiang Lin. “Deep learning based automated diagnosis of bone metastases with SPECT thoracic bone images.” In: *Scientific Reports* (2021).
- [62] Kaiming He et al. “Deep Residual Learning for Image Recognition.” In: *Proceedings of the IEEE Conference on Computer Vision and Pattern Recognition (CVPR)*. 2016, pp. 770–778.
- [63] Nicolaou et al. “An Explainable AI Model in the Assessment of Multiple Sclerosis Using Clinical Data and Brain MRI Lesion Texture Features.” In: *Journal of Medical Imaging and Radiation Oncology* 67 (2023), pp. 115–123.
- [64] Cruciani et al. “Explainable 3D-CNN for Multiple Sclerosis Patients Stratification.” In: *NeuroImage* 224 (2021), p. 117422.
- [65] Raab et al. “A Multimodal 2D Convolutional Neural Network for Multiple Sclerosis Lesion Detection.” In: *Neuroinformatics* 18 (2020), pp. 391–403.
- [66] Raab et al. “Investigation of an Efficient Multi-modal Convolutional Neural Network for Multiple Sclerosis Lesion Detection.” In: *Journal of Neuroscience Methods* 373 (2023), p. 109758.
- [67] Kim et al. “Multimodal Image Analysis for Assessing Multiple Sclerosis and Future Prospects Powered by Artificial Intelligence.” In: *Journal of Medical Imaging* 7.4 (2020), p. 044501.
- [68] Khattap et al. “Advancing Multiple Sclerosis Diagnosis Through an Innovative Hybrid AI Framework Incorporating Multi-view ResNet and Quantum RIME-Inspired Metaheuristics.” In: *Artificial Intelligence in Medicine* 135 (2025), p. 102398.

Bibliography

- [69] Statsenko et al. “Multimodal Diagnostics in Multiple Sclerosis: Predicting Disability and Conversion from Relapsing-Remitting to Secondary Progressive MS – Protocol for Systematic Review and Meta-Analysis.” In: *Systematic Reviews* 12.1 (2023), p. 134.
- [70] Selvaraju et al. “Grad-CAM: Visual Explanations from Deep Networks via Gradient-based Localization.” In: *Proceedings of the IEEE International Conference on Computer Vision (ICCV)*. 2017, pp. 618–626.
- [71] Moein Amin et al. “Artificial Intelligence and Multiple Sclerosis.” In: *Current Neurology and Neuroscience Reports* (2024).
- [72] Kearns et al. “FutureMS Cohort Profile: A Scottish Multicentre Inception Cohort Study of Relapsing-Remitting Multiple Sclerosis.” In: *Multiple Sclerosis Journal* 28.5 (2022), pp. 647–656.
- [73] Rehák Bučková et al. “Multimodal-neuroimaging machine-learning analysis of motor disability in multiple sclerosis.” In: *Brain Imaging and Behavior* 17 (2023), pp. 18–34.
- [74] Rondinella et al. “Boosting multiple sclerosis lesion segmentation through attention mechanism.” In: *Computers in Biology and Medicine* 161 (2023).
- [75] Al-iedani et al. “Multi-modal Neuroimaging Signatures Predict Cognitive Decline in Multiple Sclerosis: A 5-Year Longitudinal Study.” In: *Journal of Neuroscience* 44.3 (2024), pp. 567–579.
- [76] Anderhalten et al. “Emerging MRI and Biofluid Biomarkers in the Diagnosis and Prognosis of Multiple Sclerosis.” In: *Frontiers in Neurology* 15 (2024), p. 114.
- [77] Magi Andorraet al. “Predicting disease severity in multiple sclerosis using multi-modal data and machine learning.” In: *Journal of Neurology* 271.3 (2024), pp. 1133–1149.
- [78] Lee et al. “BioBERT: a pre-trained biomedical language representation model for biomedical text mining.” In: *Bioinformatics* 36.4 (2020), pp. 1234–1240.
- [79] Isensee et al. “nnU-Net: a self-configuring method for deep learning-based biomedical image segmentation.” In: *Nature Methods* 18 (2021), pp. 203–211.

Webography

- [80] Multiple Sclerosis International Federation. *Atlas of MS 2023*. 2023. URL: <https://www.msif.org/news/2023/08/21/new-prevalence-and-incidence-data-now-available-in-the-atlas-of-ms/>.
- [81] Genentech Biotechnology corporation. *Multiple Sclerosis*. 2021. URL: <https://www.gene.com/patients/disease-education/multiple-sclerosis>.
- [82] Roberto Alejandro M. *How to do Bias Field Correction with Python*. 2023. URL: <https://medium.com/@alexandro.ramr777/how-to-do-bias-field-correction-with-python-156b9d51dd79>.
- [83] M. K. Gurucharan. *Basic CNN Architecture: A Detailed Explanation of the 5 Layers in Convolutional Neural Networks*. Accessed: 07/05/2025. 2025. URL: <https://www.upgrad.com/blog/basic-cnn-architecture/>.